4/4/2025

Early flowering and hyperaccumulation in *Noccaea caerulescens*

A versatile tool to knock out FLC, and bzip19 causes lower uptake of Ni and Cd in Noccaea caerulescens

Margreet Blankestijn

March 2025
MSc Thesis report

WAGENINGEN
UNIVERSITY & RESEARCH

Title:	A versatile tool to knock out *FLC,* and *bzip19* causes lower uptake of Ni and Cd in *Noccaea caerulescens*
Name:	Margreet Blankestijn
Registration number:	1003081
Study:	MSc Biology
Specialization:	A) Cell Biology and Molecular Interactions
Chair group:	Laboratory of Genetics
Course code:	GEN80436
Date:	04/04/2025
Daily supervisors:	Ai Lin & René Boesten
Examiners:	René Boesten & Mark Aarts

Abstract

Hyperaccumulating plants can give insights into genetic pathways that can be targeted for biofortification of foods to mitigate micronutrient deficiency of for example Zn, and can furthermore aid in remediating polluted soil, perhaps even with the option of phytoextraction of more precious elements, like Ni and Cd. The Zn, Ni and Cd hyperaccumulating species *Noccaea caerulescens* serves as an interesting model, due to differences in hyperaccumulation and hypertolerance properties between accessions, allowing comparisons between similar genetic backgrounds. One of the current limitations decreasing the efficiency of genetic studies, the long generation time of *N. caerulescens*, was addressed here. I successfully transformed *Agrobacterium tumefaciens* with a vector containing a CRISPR-Cas9 construct and two sgRNAs targeting *FLC* exon 1 that can be used in a broad range of *N. caerulescens* accessions to generate early flowering lines. Moreover, to further understand Zn, Ni and Cd hyperaccumulation, *bZIP19*, the key in the Zn deficiency response in *Arabidopsis thaliana*, was targeted to determine the effect of a *bzip19* knock out in the hyperaccumulating context of *N. caerulescens*. Here I show that Ni and Cd uptake is lower in *bzip19* mutants compared to *bZIP19* wildtypes, whereas Zn appears to be less affected. The decrease in Ni and Cd uptake suggests that at least some of the target genes of bZIP19 are responsible for part of the hyperaccumulation of Ni and Cd in *N. caerulescens*. Furthermore, the apparent unaffected Zn concentrations, might indicate the presence of a backup system to maintain Zn hyperaccumulation. Understanding the effect of *bzip19* on the expression of the target genes and how the target genes affect Zn, Ni and Cd uptake can give valuable insights into hyperaccumulation in *N. caerulescens* that may be applied in crop species in the future.

Table of Contents

1. Introduction

One of the global challenges faced today is the prevalence of micronutrient deficiency, not only in underdeveloped regions, but also increasingly in the developed world (Hussain *et al.*, 2022; Sharma *et al.*, 2012). An unbalanced diet relying primarily on a single cereal like rice, containing a low amount of bioavailable iron (Fe) and zinc (Zn), can give rise to deficiencies in these micronutrients (Bouis & Welch, 2010; Sharma *et al.*, 2012). The micronutrient Zn is an important metal for all living organisms. For instance, the proteome of eukaryotes contains between 8%-10% Zn (Andreini *et al.*, 2006). Zn is found in all six enzyme classes, in which Zn functions in the catalytic domain or in stabilizing the structure of proteins (Andreini *et al.*, 2006; Andreini & Bertini, 2012). In humans, Zn deficiency can give rise to a plethora of health issues, including decreased immune system functioning, decreased neurobehavioral development, and diarrhea (Holtz & Brown, 2004; Roohani *et al.*, 2013; Sharma *et al.*, 2012). There are various ways to mediate Zn deficiency, like changes in diet or the commercial fortification of food using supplements. However, these options to combat Zn deficiency are not always readily available, especially to more underdeveloped regions (Roohani *et al.*, 2013). A potentially attractive alternative to combat the ongoing problem of Zn deficiency in humans is by making genetically enhanced foods with increased levels of micronutrients, also known as biofortification (Kumar *et al.*, 2019; Roohani *et al.*, 2013).

Another current challenge is soil contamination by excess levels of metals like Zn, nickel (Ni) or cadmium (Cd). Soil contamination is caused by anthropogenic activities, like prolonged exposure of soil to metal smelters (Haider *et al.*, 2021; Li *et al.*, 2015), excessive use of fertilizers (Haider *et al.*, 2021; Kaur *et al.*, 2024; Khan & Wen, 2020), or mining (Guo *et al.*, 2021; Haider *et al.*, 2021). Not only can high soil levels of Zn, Ni and Cd have adverse effects on human health (Genchi *et al.*, 2020a; Genchi *et al.*, 2020b; Li *et al.*, 2021; Schoofs *et al.*, 2024), but high Zn, Ni and Cd in soils can also cause growth problems in intolerant plant species (Haider *et al.*, 2021; Natasha *et al.*, 2022; Rizwan *et al.*, 2024). Firstly, excess Zn in plants can lead to chlorosis or even necrosis, caused by a decrease in V-ATPase levels (Fakao *et al.*, 2011). Secondly, overall plant growth is also lower under high Zn conditions, possibly due to reduced nicotinamide levels, speeding up NAD^+ degradation, which lowers the overall energy metabolism (Zhang *et al.*, 2017). Thirdly, Zn stress can inhibit root growth, decreasing total root area and thereby lowering the uptake of water or other nutrients (Kaur & Garg, 2021). Ni- and Cd-stress can cause various issues in plants, for example related to photosynthesis, seed germination, or nutrient uptake and results in chlorosis (Haider *et al.*, 2021; Rizwan *et al.*, 2024). Taken together these symptoms can be devastating for plants and can ruin harvests.

The Zn, Ni and Cd contamination can be remediated using Zn, Ni or Cd hyperaccumulating plant species as a natural way to remove the excess Zn, Ni and Cd from the soil, a process known as phytoremediation (Zou *et al.*, 2021). A hyperaccumulator is defined as an organism that can take up at least 1000 times more of an element compared to non-hyperaccumulators (Lin *et al.*, 2016). Polluted sites may even be exploited for phytomining. In phytomining, the accumulated levels of metal in the shoots of plants are harvested (Fadzil *et al.*, 2024). Phytomining is more efficient when biomass is greater. Therefore developing genetically modified plants with an increased affinity for the uptake of desirable elements, such as Ni, in species with high biomass production may increase the economic benefits of phytomining (Dang & Li, 2021). Zn, Ni or Cd hyperaccumulator species can be used and may provide insights into potential target genes for genetic modification to increase Zn, Ni or Cd uptake in other species or enhance affinity within the hyperaccumulating species.

A commonly used model species for Zn, Ni and Cd hyperaccumulation is *Noccaea caerulescens*, formerly known as *Thlaspi caerulescens* (Pollard *et al.*, 2014). *N. caerulescens*

is a diploid plant that is part of the Brassicaceae family. A total of six genetically diverse subgroups are present within *N. caerulescens* (Yamjabok *et al.*, 2024). As a facultative metallophyte, *N. caerulescens* can grow on both metalliferous and non-metalliferous soils, as opposed to obligate species which require metalliferous soils (Pollard *et al.*, 2014). *N. caerulescens* can hyperaccumulate Zn, Cd, lead and Ni (Pollard *et al.*, 2014; Wang *et al.*, 2020) and is widespread throughout Europe occurring in various types of soils, ranging from high Zn, Ni, or Cd concentrations to nonmetalliferous soils (Sterkeman *et al.*, 2017). *N. caerulescens* is a favorable model for hyperaccumulation, because of the differences in hyperaccumulation and hypertolerance properties within the species (Halimaa *et al.*, 2014). Local adaptation to differing soil conditions gives rise to a natural variation of the genome. Some, but not all accessions are hyperaccumulators and some, but not all accessions are hypertolerant, allowing for comparisons of these traits within similar genetic backgrounds (Halimaa *et al.*, 2014). Furthermore, a method to genetically modify *N. caerulescens* was developed (Yamjabok *et al.*, 2024), making genetic studies more feasible.

One of the current limitations in doing genetic research using *N. caerulescens* is its long generation time. All known natural accessions of *N. caerulescens* need a vernalization period (Peer *et al.*, 2003). The vernalization period is around 2.5 months and the total growth cycle per generation is around 7 months (Wang *et al.*, 2022). A successful transformation method for *N. caerulescens* relies on *Agrobacterium tumefaciens* mediated flower dipping (Yamjabok *et al.*, 2024). However, due to *N. caerulescens'* long vernalization period and therefore long generation time, the efficiency of genetic studies utilizing *Agrobacterium tumefaciens* mediated flower dipping is lower, compared to for example *Arabidopsis thaliana*. One way to shorten the generation time of *N. caerulescens* is by making early flowering mutants (Wang *et al.*, 2020). FLOWERING LOCUS C (FLC) and SHORT VEGETATIVE PHASE (SVP) are important regulators of flowering initiation by repressing downstream genes (Kim & Sung, 2014; Wang *et al.*, 2020). VERNALIZATION INSENSITIVE 3 (VIN3) is induced after a vernalization period and downregulates *FLC* in *A. thaliana* (Kim & Sung, 2014). Downstream genes, like *FLOWERING LOCUS T* (*FT*) and *SUPPRESSOR OF OVEREXPRESSION OF CO 1* (*SOC1*), which are responsible for meristem transitioning from vegetative to floral state, will no longer be repressed by FLC after vernalization (Fig. 1.1) (Kim & Sung, 2014; Wang *et al.*, 2020). When *FT* and *SOC1* are no longer inhibited a shift from vegetative to floral state is initiated (Kim & Sung, 2014; Wang *et al.*, 2020). A similar, but not identical, mechanism controlling flowering is present in *N. caerulescens* compared to *A. thaliana* (Fig. 1.1) (Wang *et al.*, 2020). Vernalization of *N. caerulescens* also represses *FLC*, but no involvement of VIN3 has been reported thus far (Wang *et al.*, 2020). SVP was not found to be significantly affected by a vernalization period in *N. caerulescens*, but instead an effect of photoperiod was suggested (Wang *et al.*, 2020). FLC and SVP form a complex, suggesting that flowering may still be induced if only one of the two genes is knocked out (Mattheos *et al.*, 2015). Indeed, a mutation in either *FLC* or *SVP* will cause earlier flowering that is not dependent on vernalization both in *A. thaliana* and in *N. caerulescens* (Kim & Sung, 2014; Wang *et al.*, 2020). SVP not only regulates flowering, but is also linked to for example temperature-dependent functions (Lee *et al.*, 2007) and drought-stress (Bechtold *et al.*, 2016), indicating that knocking out *SVP* might have unwanted pleiotropic effects. Therefore, the focus of this study will be on *FLC.* Previously, an *flc* mutant with an early flowering phenotype has been generated via Ethyl methanesulfonate-induced mutagenesis (Wang *et al.*, 2020; Yamjabok *et al.*, 2024). This early flowering line can be introgressed into another genetic background and selfed for several generations to create a homozygous mutant of *flc* (Yamjabok *et al.*, 2024). However, introgression is a lengthy process (Reed & Bargmann, 2021) and the background alleles may still segregate and may vary per progeny, since a cross is made between different accessions

that are not fully homozygous in this method. Knocking out *FLC* via CRISPR-Cas 9 would make obtaining different early flowering lines faster, as less rounds of selfing are needed, and would ensure an isogenic background. A common CRISPR construct can be created that can knock out *FLC* in various genetic backgrounds, since *FLC* contains a highly conserved DNA-binding MADS domain (Gramzow *et al.*, 2023). Once established, the CRISPR tool can be used to make early flowering lines of various accessions. I aim to produce such a versatile tool to knock out *FLC* in various *N. caerulescens* accessions, to allow for faster comparisons of accessions with differences in hyperaccumulation and hypertolerance properties.

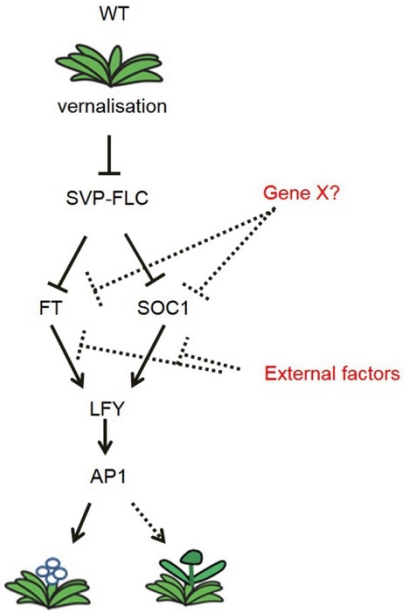

Figure 1.1 Proposed model of flowering time regulatory pathway in *N. caerulescens*.

Upon vernalization *SVP* and *FLC* are repressed. This releases the suppression of *FLC* and *SVP* on the genes *FLOWERING LOCUS T* (*FT*) and *SUPPRESSOR OF OVEREXPRESSION OF CO 1* (*SOC1*). The release of suppression of *FT* and *SOC1* leads to a cascade that will induce flowering. An unknown gene X is suggested to also inhibit *FT* and *SOC1*, as portrayed by the dotted line. Moreover, external factors, like temperature or photoperiod may also play a role. (Wang *et al.*, 2020)

Besides using CRISPR-Cas9 to create early flowering *N. caerulescens* lines, it is also possible to use an early flowering accession to introgress this trait into another background. A Clough wood *N. caerulescens* line with an introgressed *flc* mutation of the Saint Felix de Pallières accession was genetically modified to knock out *bZIP19* (Lin, 2023; Vijverberg, 2022). Two transcription factors from the basic leucine zipper (*bZIP*) family, bZIP19 and bZIP23, are master regulators of the Zn deficiency response of the non-hyperaccumulator model *A. thaliana* (Ana *et al.*, 2010; Lilay *et al.*, 2019; Lilay *et al.*, 2021). bZIP transcription factors contain a basic DNA binding region, indicating a gene regulatory function, and a leucine zipper, which allows dimerization (Stolz & McCromick, 2020). bZIP19 and bZIP23 can bind to Zn^{2+} ions via a Cysteine/Histidine-rich motif called the Zn-sensing motif (ZSM) (Lilay *et al.*, 2021). When low levels of Zn are present, the ZSM will mostly not be bound to Zn and bZIP19 and bZIP23 is then able to dimerize (Fig. 1.2A) (Lilay *et al.*, 2021). The dimer will bind to an imperfect palindromic region of 10 base pairs, called the Zn deficiency response element (Assunção *et al.*, 2010a). Upon binding, the bZIP dimer activates the Zn deficiency response element promotor, upregulating the transcription of various downstream genes, including various other ZIP-genes and *NICOTIANAMINE SYNTHASE 2* and *4* (Assunção *et al.*, 2010a; Assunção *et al.*, 2010b; Lilay *et al.*, 2019). The downstream genes

of bZIP19 and bZIP23 regulate the uptake of Zn in the roots and translocation of Zn throughout the plant (Assunção *et al.*, 2010a). Once a Zn sufficient state is reached, Zn will bind to the ZSM of bZIP19 and bZIP23, due to which bZIP19 and bZIP23 will no longer dimerize, deactivating the transcription inducing function of bZIP19 and bZIP23 (Fig. 1.2B) (Lilay *et al.*, 2021). The binding of Zn to the ZSM will therefore halt the transcription of genes facilitating Zn uptake and translocation, making the Zn deficiency response a negative feedback loop (Lilay *et al.*, 2021). However, if a mutation occurs in the ZSM, Zn^{2+} can no longer bind, causing bZIP19 and bZIP23 to be constitutively active (Lilay *et al.*, 2021). Downstream genes are then constitutively promoted by bZIP19 and bZIP23 causing a continuous uptake of Zn (Fig. 1.2C) (Lilay *et al.*, 2021). Some of the downstream genes of bZIP19 and bZIP23, like *ZIP-LIKE ZINC TRANSPORTER 1* (*ZNT1*), show low-affinity uptake of Cd and of Ni, besides a high-affinity uptake of Zn (Deng *et al.*, 2017; Lin *et al.*, 2016). bZIP19 and bZIP23 are highly conserved throughout evolution, suggesting a similar function in the Zn deficiency response in *N. caerulescens* (Castro *et al.*, 2017; Vijverberg, 2022). Although bZIP23 is very conserved across all plants, bZIP23 appears to be deleted in the *N. caerulescens* accessions Clough Wood and Le Blémard, whereas it is present in the accession Ganges (Lin, 2023). For other *N. caerulescens* accessions it is not known if bZIP23 is present. Moreover, why bZIP23 was lost in evolution and how this affects the Zn homeostasis is not yet known. The function of bZIP19 is not yet clear within the hyperaccumulating context of *N. caerulescens*, but may give insights into the genetic pathways behind the hyperaccumulation of Zn, Ni and Cd.

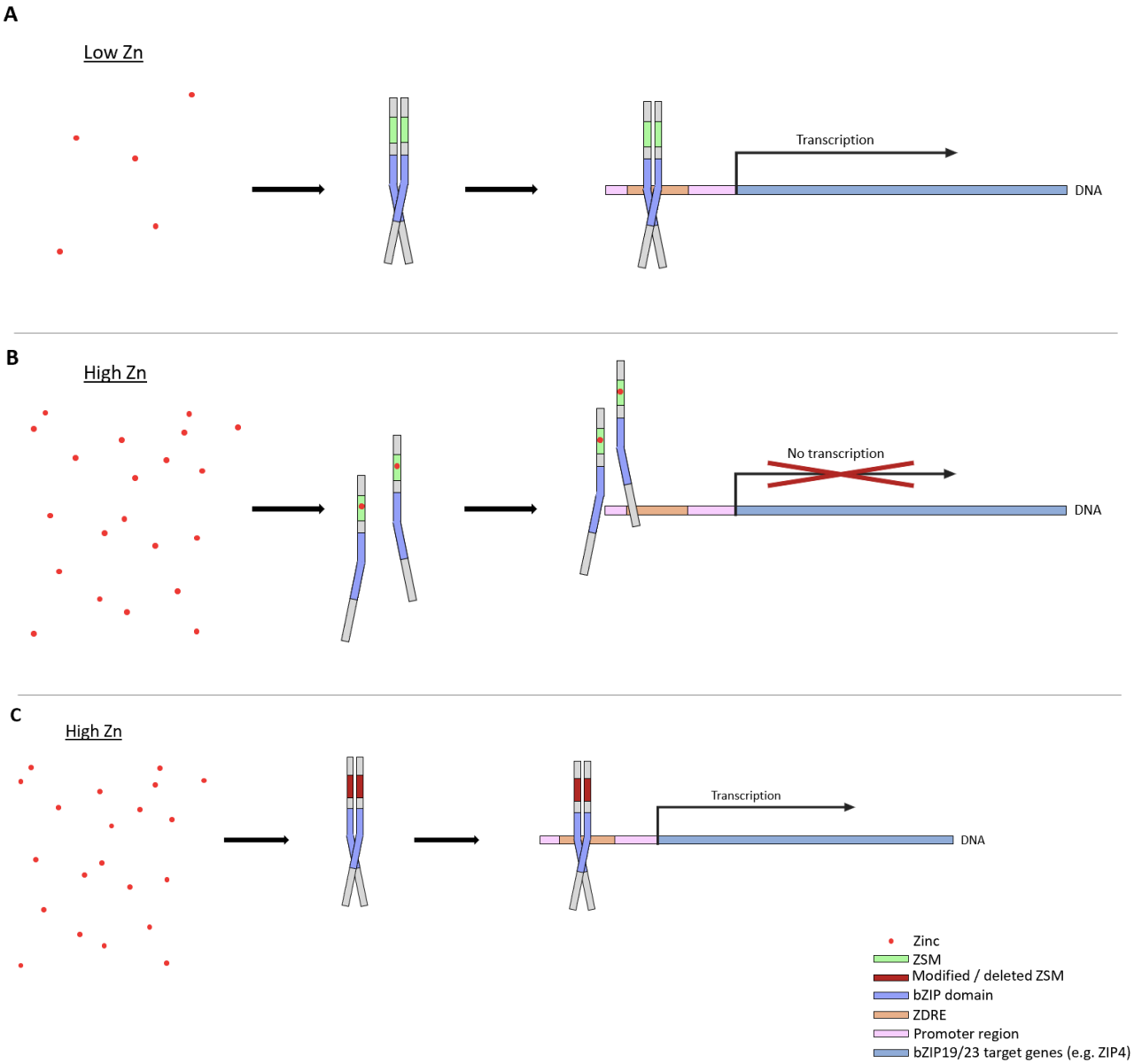

Figure 1.2 Zinc sensing in *Arabidopsis thaliana* via bZIP19 and bZIP23.

A) When low levels of zinc are present, little zinc will bind to the zinc-sensing region of the bZIP. When no zinc is bound dimers can form, that can bind to the promotor of the target gene, thereby promoting transcription. B) In zinc sufficient conditions zinc will bind to the zinc-sensing motif. The bZIP will not promote transcription of target genes in zinc sufficient conditions. C) If the zinc-sensing motif is disrupted, zinc will no longer bind to the zinc sensing motif of the bZIP. This will cause a constitutive promotion and thereby transcription of target genes by bZIP19 and bZIP23 causing zinc accumulation. (Lilay et al., 2019; Lilay et al., 2021) (Image retrieved from Vijverberg, 2022)

The goal of this thesis is to determine the effect of bZIP19 on the levels of Zn, Ni and Cd hyperaccumulation in *N. caerulescens*. I will measure the amount of Zn, Ni or Cd that is accumulated in a *bzip19* Clough Wood *N. caerulescens* accession. I hypothesize that Zn concentrations will be lower in a *bzip19* plant compared to a *bZIP19* plant, because I expect that the downstream genes of bZIP19 will not be upregulated when *bZIP19* is knocked out, regardless of the Zn conditions (Fig. 1.3). Consequently, the roots will not upregulate the intake of Zn, as no proteins aiding in the uptake of Zn from the growing medium will be produced, resulting in a lower intake of Zn in roots. The reduction of uptake of Zn by roots is expected to lead to decreased Zn levels in the shoots of *N. caerulescens*. I further hypothesize

that Ni and Cd levels will be lower in a *bzip19* mutant compared to *bZIP19*, as some of the Zn uptake genes regulated by bZIP19 can also take up Ni and Cd with lower affinity. Therefore, I hypothesize that *N. caerulescens* will show lower levels of Zn, Ni and Cd, in both shoots and roots in a *bzip19* mutant compared to a wildtype *bZIP19*, assuming that *bZIP19* is the key regulator of Zn uptake in *N. caerulescens*.

To conclude, in this thesis a versatile CRISPR tool to create early flowering *N. caerulescens* lines in various genetic backgrounds will be made, the effect of knocking out *bZIP19* on the hyperaccumulation of Zn, Ni and Cd will be determined and a knockout of the ZSM in *bZIP19* will be made.

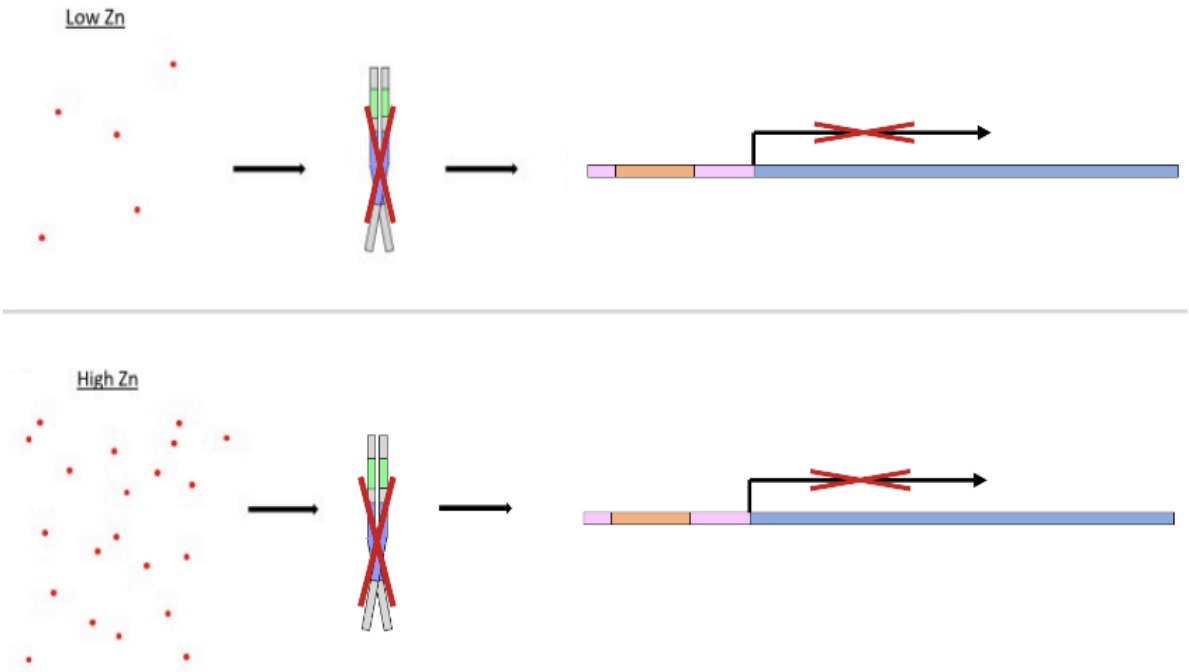

Figure 1.3 Hypothesized model for a full knock out of *bZIP19* in *Noccaea caerulescens*.

If *bZIP19* is knocked out no bZIP19 is present to sense zinc levels. Therefore, irrespective of zinc concentration, the downstream genes of bZIP19 will never be upregulated.

2. Materials and Methods

2.1 Generation of a versatile tool to knock out *FLC* in various genetic backgrounds in *Noccaea caerulescens*

FLC across accessions in *Noccaea caerulescens*

Primer design

To knock out *FLC* in various accessions of *N. caerulescens* two sgRNAs were designed. The Ganges genome was used as a reference to design the sgRNAs (Appendix 1). *FLC* exon 1 was the target of both of the sgRNAs. Possible target sites must include a downstream PAM site (5'-NGG-3'). No recognition sites of any of the type-II restriction enzymes that were used (BpiI and BsaI) in the Golden Gateway cloning may be present in the target site and the sgRNAs must be unique in the genome. The uniqueness of the sequences was validated using BLASTn (Geneious Prime). The GC content should be at least 40%. A sticky end overhang, corresponding to the cut site of the type-II restriction enzyme BpiI, was added to the sgRNA at the 5'-end allowing ligation into the shuttle vector.

Selection of accessions

To determine the applicability of the designed sgRNAs in the context of different genetic backgrounds within *N. caerulescens*, the DNA of a broad range of *N. caerulescens* was isolated. Building upon a previous selection of accessions, that was based on the ability to produce high numbers of seeds and the ability to self-fertilize (Yamjabok *et al.*, 2024), I selected some additional accessions to have an approximately even selection of accessions over all six subgroups present within *N. caerulescens* (Fig. 2.1).

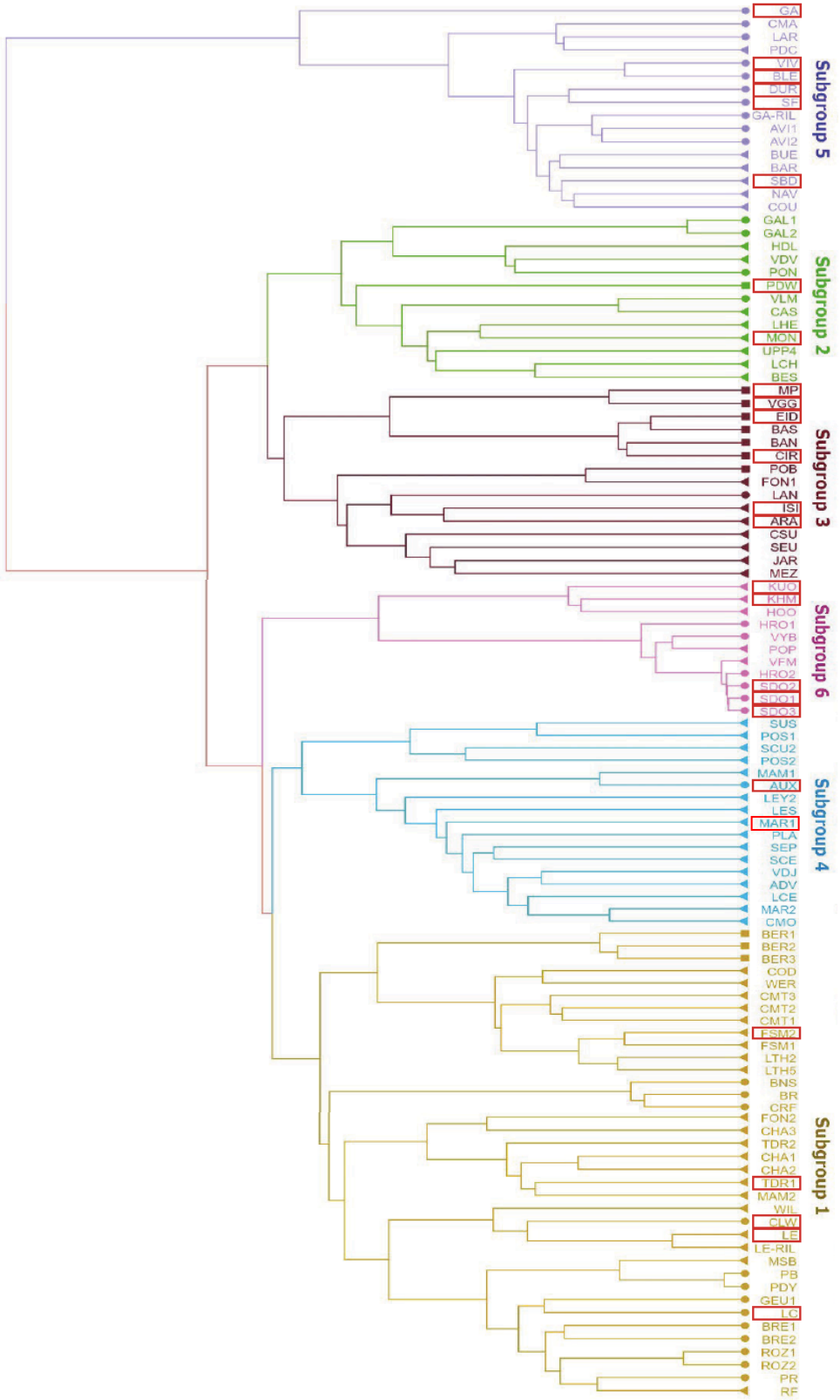

Figure 2.1 Phylogenetic tree of *N. caerulescens* showing the six subgroups and the selection of accessions used for DNA isolation.

Accessions in red boxes were used for DNA isolation to determine the DNA sequence of *FLC* exon 1. (Yamjabok *et al.*, 2024)

Growing conditions N. caerulescens accessions

Seeds of 28 accessions (Appendix 2) were sterilized as described under section 2.2 “Plant material and growing conditions” and sown on agar plates by Nick Olivier and Corrie Hanhart (Olivier, 2025). Seedlings were transferred to pots containing a substrate provided by Nergena and grown for several weeks before harvest.

DNA isolation

Young leaf material was collected in 1.5 mL screwcap Eppendorf tubes containing three to four glass beads of 3 mm and frozen in liquid nitrogen immediately after harvesting. Samples were temporarily stored at – 80 °C until DNA isolation. While maintaining freezing temperatures, samples were ground using a RETSCH Mixer Mill MM400 at 30 Hz for two minutes. Once finely ground, 500 µL CTAB buffer (2% CTAB, 1.4 M NaCl, 100 mM Tris pH=8, 20 mM EDTA) was added. Samples were vortexed shortly and thereafter incubated in a water bath at 65 °C for 30 minutes. The samples were then left to cool down to room temperature in a fume hood before adding 500 µL chloroform:isoamylalcohol (24:1). Samples were vortexed and centrifuged for 15 minutes at 3250 rpm. The top phase was mixed with 300 µL ice-cold isopropanol in a new 1.5 mL Eppendorf tube. The Eppendorf tubes were kept at – 20 °C overnight. The next day the samples were centrifuged for 15 minutes at 3250 rpm and the supernatant was discarded. 200 µL ethanol was added, samples were vortexed and centrifuged for 5 minutes at 3250 rpm. The previous step was performed twice. After the second time the ethanol was poured out and tubes were left for at least 30 minutes in the fume hood to let remaining ethanol evaporate. Lastly, the remaining pellet was dissolved in 50 µL milli-Q water. A gel electrophoresis, with 1% agarose containing ethidium bromide, was performed to get an indication on the concentration of isolated DNA. Moreover, the DNA concentration of the isolated DNA was determined using a DeNovix DS-11 FX Spectrophotometer/Fluorometer.

Gene amplification and sequencing

To amplify *FLC* exon 1 a PCR was performed using PCRBIO VeriFi™ Mix Red. Both primer pairs were first tested on the GA and CLW accessions. After a successful test all isolated *N. caerulescens* DNA was used to perform the PCR, to amplify *FLC* exon 1. Genomic DNA was diluted to a concentration of 60-100 ng. 1 µL diluted DNA was mixed with 1 µL of 10 µM forward primer, 1 µL of 10 µM reverse primer one (Table 2.1) and 12.5 µL 2x PCRBIO VeriFi™ Mix Red (PCRBIO VeriFi™ Polymerase, 6 mM $MgCl_2$, 2 mM dNTPs, enhancers, stabilizers, red dye). The cycle conditions used in the PCR were adapted from PCRBIO VeriFi™ (Table 2.2). The PCR product was loaded on an agarose electrophoresis gel for a visual validation of successful amplification. As a negative control, the PCR was performed using milli-Q water instead of a DNA template and the previously tested CLW genetic background was used as an additional control to verify successful cycling conditions. Unsuccessful amplifications were repeated using reverse primer two (Table 2.1).

Table 2.1 Primers amplifying *FLC* exon 1 in *Noccaea caerulescens*.

Primer pair 1 contains the forward primer and reverse primer 1. Primer pair 2 contains the forward primer and reverse primer 2.

Primer name	Sequence (5' to 3')
FLC_PCR_fw	ATCTCATGTATCTCTCATGGCCAT
FLC_PCR_rev1	GCGTGGATGTCTTGTCGTTA
FLC_PCR_rev2	GCCCACGCGTAATTCGTCATGC

Table 2.2 Cycle conditions for the PCR amplifying *FLC*.

Cycles	Temperature	Time
1	95 °C	1 minute
35	95 °C	15 seconds
	60 °C	15 seconds
	72 °C	1 minute
1	72 °C	5 minutes
-	12 °C	Infinite

The amplicon resulting from the PCR reaction was send to Eurofins genomics for Sanger sequencing. The PCR product was diluted ten times and 5 µL of this dilution together with 5 µL of 5 uM forward primer was send for Sanger sequencing. Sequences were aligned using the MAFFT alignment on the online website Benchling.

Development of transformation vector containing CRISPR-Cas9 with sgRNA for *FLC*

Isolation of vector backbone

Escherichia coli cells containing vector backbones with CRISPR-Cas9 construct, but without sgRNAs (pDGE331 (M1), pDGE334 (M2E), pDGE347 (recipient vector)) were provided by Wageningen University & Research. (Appendix 3)

The glycerol stocks containing *E. coli* containing the empty M1 and M2E shuttle vectors were spread on selective LB plates (10 g Bacto-Tryptone, 5 g Bacto-Yeastextract, 10 g NaCl, 8 g Micro-agar, demi-water to a total volume of 1 L) containing Carbenicillin (100 ug/mL) and the recipient vector was spread on selective LB plates containing Spectinomycin (100 ug/mL). Plates were incubated at 37 °C for 16 hours. Three single colonies were inoculated in separate tubes containing 3 mL selective LB medium without Micro-agar (Carbenicillin 100 ug/mL for M1 and M2E, Spectinomycin 100 ug/mL for recipient vector) and incubated at 37 °C for 16 hours. 1.5 mL of the incubated mixture was transferred to a 2 mL Eppendorf tube and spun down for 1 minute at max rpm. The supernatant was removed. Plasmids were then isolated using the Nucleospin Plasmid EasyPure miniprep kit (Macherey-Nagel). The DNA concentration was measured with a Qubit using the broad range dsDNA quantification assay kit. The isolated vector backbone was visualized on a 1% agarose gel electrophoresis with ethidium bromide, to get an indication on the size of the vector. The size of the vector was compared with a previously verified vector of the same size. Plasmids showing the same size as the reference plasmid were presumed to be the correct plasmid.

Generation of intermediary shuttle vectors

To generate the intermediary shuttle vectors (Fig. 2.2), the sgRNA oligonucleotides were first hybridized using an annealing buffer (10 mM Tris pH 7.5-8.0, 1 mM EDTA, 50 mM NaCl) to make a final concentration of 10 µM sgRNA. The oligonucleotides in annealing buffer were heated to 98 °C for 5 minutes and slowly cooled down to room temperature. 20 fmol (or 60 ng) of isolated empty shuttle vector was combined with 50 fmol hybridized sgRNA, 1 µL 10X Ligation buffer (New England Biolabs), 0.1 µL 10X BSA (10 mg/mL) (New England Biolabs), 0.3 µL BpiI restriction enzyme (Thermo Scientific), 0.1 µL T4 DNA Ligase (3 u/µL) (New England Biolabs), and milli-Q water to a total volume of 10 µL and the total mixture was subjected to the temperature cycles as shown in table 2.3. sgRNA1 was combined with shuttle vector M1 and sgRNA2 was combined with shuttle vector M2E (Fig. 2.2). (Stuttmann *et al.*, 2021)

Table 2.3 Cycle conditions for the digestion ligation reaction of the shuttle vectors.

Cycles	Temperature	Time
30	37 °C	2 minutes
	16 °C	5 minutes
1	50 °C	10 minutes
1	80 °C	10 minutes
-	12 °C	Infinite

Heat shock transformation of E. coli

To amplify the vector DNA, *E. coli* was transformed. Of the assembled shuttle vector 10pg-100ng was gently mixed with 25 µL competent TopTen *E. coli* cells. After 5-15 minutes on ice the *E. coli* cells were given a heat shock by placing them in a thermoblock at 42 °C. After 45 seconds the shocked cells were immediately placed back on ice for 5 minutes. Subsequently, 1 mL of LB medium was added and cells were incubated at 37 °C for 1 hour, while shaking at 250 rpm. After incubation the cells were spun down and approximately 50 µL of the supernatant was kept. Cells were then resuspended in the remaining supernatant and were plated on selective LB agar plates (100 ug/mL Carbenicillin). Incubation and isolation of the plasmid, as well as DNA concentration measurements and gel electrophoresis were performed as described under "Isolation of vector backbone". As a control the empty M1 plasmid was used in the gel electrophoresis. Moreover, to verify the correct insertion of the full sgRNA, the isolated plasmids that showed the desired pattern on the agarose gel were send for Sanger sequencing to Eurofins Genomics. 5 µL of plasmid DNA with a concentration of 60-150 ng/µL was mixed with 2.5 µL of 10 uM reverse primer (sgRNA_RBOHF_R2: AAACCCAGCACCGCCGCTTTGATT) and 2.5 µL milli-Q water for Sanger sequencing. The sequence was aligned to the expected M1 or M2E shuttle vector using the program ApE.

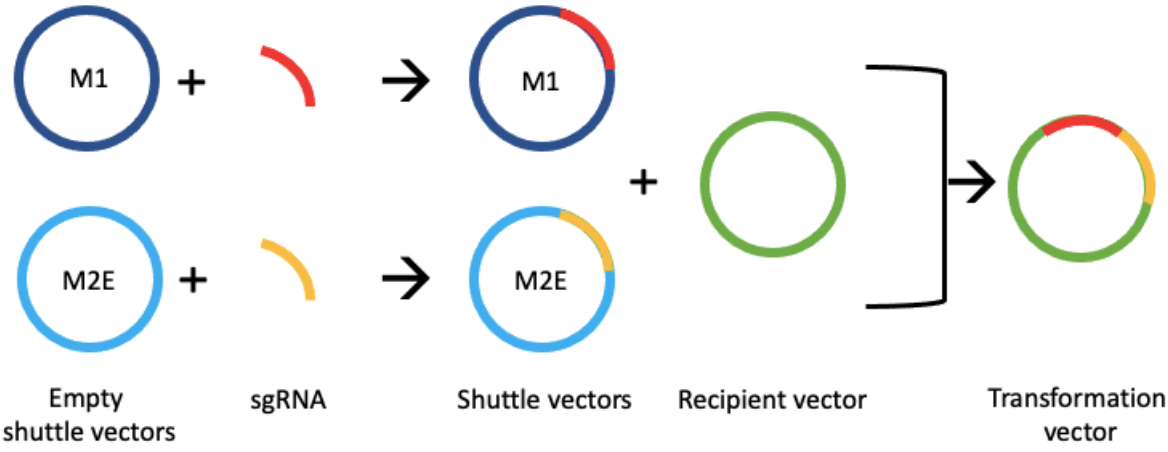

Figure 2.2 Workflow of the Golden Gateway cloning process followed to get the final transformation vector containing a CRISPR-Cas9 construct with an sgRNA targeting *FLC* exon 1 in *N. caerulescens*.

Generation of transformation vector

To generate the final transformation vector, 20 fmol (or 300 ng) of isolated empty recipient vector was combined with 20 fmol (or 40 ng) of both shuttle vector M1 and M2E, 2 µL 10X Ligation buffer (New England Biolabs), 0.2 µL 10X BSA (10 mg/mL) (New England Biolabs), 1 µL BsaI restriction enzyme (New England Biolabs), 1 µL T4 DNA Ligase (3 u/µL) (New England Biolabs), and milli-Q water to a total volume of 20 µL and the total

mixture was subjected to the temperature cycles as shown in table 2.3. (Fig. 2.2) (Stuttmann *et al.*, 2021)
After generation of the transformation vector, the vector was transformed into *E. coli* following the protocol as described under "Isolation of vector backbone" with three alterations. Firstly, Spectinomycin (100 ug/mL) was used as selective antibiotic, instead of Carbenicillin. Secondly, a digestion was performed to verify the insertion of the sgRNAs. Approximately 200 ng plasmid DNA was combined with 1 µL of the restriction enzymes HindIII and PstI (New England Biolabs), 1 µL of 10X Tango Buffer (Thermo Scientific) and milli-Q water to a final volume of 10 µL. As a control the empty recipient vector was also digested. The digestion mixtures were incubated at 37 °C for 1 hour and visualized using a 1% agarose electrophoresis gel with ethidium bromide. Lastly, the whole plasmid was sequenced at PlasmidSaurus using the Standard Low Concentration category. For sequencing 10 µL of DNA with a concentration of 20-200 ng/µL was put into a PCR tube and send out. The acquired sequence was aligned to the expected sequence of the transformation vector containing both sgRNAs using the program ApE.

Transformation vector in Agrobacterium tumefaciens

The transformation vector containing both sgRNAs was transformed into *Agrobacterium tumefaciens* to be used for floral dipping in future experiments. For the transformation 100-1000 ng of plasmid DNA was added to competent *A. tumefaciens* (GV3101) and gently mixed. The cells were then incubated on ice for 5 minutes and subsequently in liquid nitrogen for an additional 5 minutes. Cells were then transferred to a water bath at 37 °C for 5 minutes. The total content was transferred to a 12 mL tube with 1 mL LB medium and incubated at 28 °C and at 200-220 rpm for 2 hours. The incubated cells were transferred to Eppendorf tubes and centrifuged for 3 minutes at 3000 rpm. The pellet was resuspended in 100-200 µL remaining LB. The resuspension was spread over two selective plates (Rifampicin 10 ug/mL, Gentamycin 100 ug/mL, Spectinomycin 100 ug/mL) using glass beads, and incubated at 28 °C for 48 hours.

Verification of Agrobacterium tumefaciens transformation

To verify the correct transformation of Agrobacterium with the transformation vector, 1.5 mL of the *A. tumefaciens* was transferred to a 2 mL Eppendorf tube and spun down for 1 minute at max rpm. The supernatant was removed. The plasmid was then isolated using the Nucleospin Plasmid EasyPure miniprep kit (Macherey-Nagel). The isolated plasmid was transformed back into *E. coli* as described under "Heat shock transformation of *E. coli*" using Spectinomycin selective plates (100 ug/mL). After isolation of the plasmid, approximately 200 ng plasmid DNA was combined with 1 µL of the restriction enzymes HindIII and PstI (New England Biolabs), 1 µL of 10X Tango Buffer (Thermo Scientific) and milli-Q water to a final volume of 10 µL. As a control the empty recipient vector and previous successful transformation vector were also digested. The digestion mixtures were incubated at 37 °C for 1 hour and visualized using a 1% agarose electrophoresis gel with ethidium bromide.
The correct M1, M2E and final transformation vector in both *E. coli* and *A. tumefaciens* were kept for long term storage in a stock of 21,5% glycerol at -80 °C.

2.2 Phenotyping *bzip19* mutant *N. caerulescens*

Plant material and growing conditions

Noccaea caerulescens seeds were provided by Wageningen Univeristy & Research. The accession Clough Wood (CLW, UK) was introgressed with a *flowering locus c* (*flc*), causing early flowering, from the St. Felix de Pallières (SF, Southern France) accession. The wildtype plants used in this study (CS7W) were self-fertilized for seven generations. *bzip19* mutant plants were produced via *A. tumefaciens* mediated transformation containing a CRISPR-Cas9

construct (Vijverberg, 2022). The selected mutant plants were self-fertilized for four generations. To correct for parental effects, seeds from three different mutant parents (CS41P1, CS41P2, CS41P3) were used in this study.

Seeds were sterilized by placing them in a desiccator in which four beakers containing a mixture of 50 mL bleach (2.5%) and 1.5 mL HCl (17.5%) were placed. Seeds were left in the desiccator for three hours and subsequently left in an active flow cabinet overnight. Sterilized seeds were then placed on bottom-cut PCR tubes containing half strength Hoagland gelrite (Table 2.1) (20 µM Zn). All half strength Hoagland was buffered at a pH of 5.5 with MES. The cut side of the PCR tubes was submerged in half strength Hoagland (20 µM Zn) to prevent drying out. A test run with 16 mutant seeds per parental type (CS41P1, CS41P2, CS41P3) was grown on 2 µM Zn and 20 µM Fe half strength Hoagland and seeds were treated with 3 µL of 100 µM Gibberellins 4+7 with potassium nitrate and stratified for one week at 4 °C. Based on the germination rate and phenotype of those mutant plants the concentration of Zn was increased to 20 µM for future trials and 40 µM Fe was added after transfer to hydroponics to prevent deficiencies before the start of treatments. Moreover, seeds were treated with 6 µL of 100 µM Gibberellins 4+7 with potassium nitrate and stratified for one week at 4 °C to induce germination. After one week the germination boxes were transferred to the hydroponics room (16hr/8hr light/dark, 21/17 °C for day/night and 70% relative humidity). Boxes were kept in sterile conditions until most seeds (≥80%) germinated or until seedlings reached the lid. After germination the boxes were opened to allow more light to reach the plants. Seedlings were transferred to hydroponics pots that could hold 700 mL liquid containing half strength Hoagland solution (20 µM Zn, 40 µM Fe) after the first/second set of true leaves had appeared. A maximum of three plants per pot was used, all of the same genotype. The Cd and Ni dosing experiment were started at the same time and a total of 26 seeds for each mutant parental line and 74 wildtype seeds were sown. For the first Zn trial 16 mutant seeds for each parental line and 48 wildtype seeds were sown. Based on the germination rate and development of the plants in the first Zn trial and the Ni and Cd experiment, 24 mutant seeds per parental line and 50 wildtype seeds were sown during a second Zn trial.

Table 2.1 Nutrient content of half strength Hoagland solution without added treatment.

Stock	Concentration (in µM)
KNO_3	3
$Ca(NO_3)_2 \cdot 4\ H_2O$	2
$NH_4H_2PO_4$	1
$MgSO_4 \cdot 7\ H_2O$	0.5
Fe(Na)EDDHA	40 (20 for germination)
1 X Micronutrients	1
$ZnSO_4 \cdot 7\ H_2O$	20
(Gelrite)	(3 g/L)

Dosing experiment conditions

Treatments were applied 24 days after sowing. The Zn dosing experiment consisted of 2 µM, 20 µM and 200 µM Zn added in the form of $ZnSO_4 \cdot 7\ H_2O$, the Ni dosing experiment consisted of 0 µM, 10 µM and 100 µM Ni added in the form of $NiSO_4 \cdot 6\ H_2O$, and the Cd dosing experiment consisted of 0 µM, 2 µM and 20 µM Cd added in the form of $CdSO_4$, all in half strength Hoagland supplemented with 20 µM Zn and 40 µM Fe. The Hoagland was completely refreshed after 14 days of treatment. Plants were harvested 46 days after sowing.

Sample preparation and measurements

Root and shoot samples were collected for future RNA isolation in 1.5 mL screwcap Eppendorf tubes containing a mixture of 2- and 3-mm glass beads. Samples were frozen in liquid nitrogen immediately after harvesting and are kept in – 80 °C for long term storage.

The remainder of the shoots and roots were dried in the oven at 65 °C for at least two days. Dry weight was determined using a Mettler Toledo balance. Samples were slightly crushed by hand and put into 2 mL Eppendorf tubes containing four 2-mm Yttria Zirconia beads. Two 3-mm Yttria Zirconia beads were added after addition of the sample. Samples were then ground in a Retch shaker at 30 Hertz for 30 seconds and/or in a Fast & Fluid paint mixer until samples were finely powdered. Around 20 mg of sample was loaded onto a film on a holder and a second film was placed on top of the sample for the Zn and Ni treatment. The elemental content of the samples was then measured using X-ray fluorescence in a JP500 Z-Spec machine. As Cd cannot be measured with the JP500 Z-Spec, these samples were sent out for ICP-AES at Université de Lorraine. Cd samples were also measured in the Z-Spec, however, in this case the weight of sample loaded onto the holder was not specified.

Data analysis

Z-Spec and dry weight data was analyzed using R Studio (version 1.4.1717). Z-Spec data was transformed into ppm and the average of technical replicates (repeated measurements of the same sample) was taken.

Normality was determined using a Shapiro-Wilk test. All samples were assumed non-normal based on the Shapiro-Wilk test and for that reason a Mann-Whitney U test was performed for all tests with $\alpha = 0.05$.

2.3 Transformation of *N. caerulescens* with CRISPR construct targeting the ZSM of *bZIP19*

A. tumefaciens cells containing a transformation vector with a CRISPR-Cas9 construct and sgRNAs targeting the ZSM of *bZIP19*, were previously generated (Lin, 2023; Vijverberg, 2022). The construct had previously been verified, but as additional validation cells were verified again as described under "Verification *Agrobacterium tumefaciens* transformation" with one modification. Instead of verifying the construct via a digestion reaction, the isolated plasmid was sent out for sequencing at PlasmidSaurus. The whole plasmid was sequenced at PlasmidSaurus using the Standard Low Concentration category. For sequencing 10 µL of DNA with a concentration of 20-200 ng/µL was put into a PCR tube and send out.

Three positive colonies were grown on selective LB medium (100 ug/mL Gentamycin, 100 ug/mL Spectinomycin, 10 ug/mL Rifampin) for two days at 28 °C. 1 mL of the culture was inoculated into 100 mL selective LB medium (100 ug/mL Gentamycin, 100 ug/mL Spectinomycin, 10 ug/mL Rifampin) and cultured at 28 °C and 250 RPM for 16-24 hours, until an optical density of 1.8-2.0 was measured. The optical density (OD_{600}) was measured using a Bio-Rad SmartSpec 3000. 50 mL of each of the colonies was then spun down for 20 minutes at 4000 RPM. The supernatant was removed and at least 25 mL of 5% sucrose was added. The solution was spun down again for 20 minutes at 4000 RPM. The pellet was resuspended in 50 mL 5% sucrose and the optical density was measured. Three final cultures of 150-200 mL with an optical density of 1.2 were made.

Thirteen Clough Wood *N. caerulescens* plants were grown in a WEISS cabinet by Ai Lin. On the day of transformation any flowers that had opened were cut off. Immediately before dipping either 0.02% or 0.05% Silwet L-77 was added to the *A. tumefaciens* colony suspensions. Part of the culture was added to a Petri dish and flowers were dipped in the culture for 5 seconds. Flowers were gently crushed during dipping for half of the plants, while the other half was not touched during dipping. After dipping a dome was put over the

transformed plants, which was removed after a few days. Seven days after the first dipping transformation the procedure was repeated. Opened flowers were not cut off during the second dipping round.

3. Results

3.1 A tool to generate early flowering lines in various *Noccaea caerulescens* backgrounds

To decrease the time needed to generate homozygous knockout plants for genetic studies, early flowering lines can be made by knocking out *FLOWERING LOCUS C* (*FLC*) in various accessions of *N. caerulescens.*

Amplification of *FLC* exon 1 in different *Noccaea caerulescens* backgrounds

The CRISPR tool is designed to work on a large selection of *N. caerulescens* accessions, as this allows the study of accessions with various levels of hyperaccumulation and hypertolerance abilities. Several criteria were used to design sgRNAs, namely: a downstream PAM sequence (5'-NGG-3'), absence of type-II restriction enzyme BpiI or BsaI target sites, at least 40% GC content, and uniqueness in the genome. Based on those criteria two CRISPR sgRNAs were designed based on a Ganges (GA) reference genome with sticky end overhangs that will allow ligation into the shuttle vector (Table 3.1). Both sgRNAs target exon 1 of *FLC* to ensure a full knock out of *FLC* and therefore complete inactivation of the FLC protein. By using two sgRNAs the efficiency of knocking out *FLC* will be increased. CRISPR-Cas9 can cut at base-pair (bp) 11 and at bp 110 after the proposed start of exon 1 (Appendix 1). If both sites are cut a deletion of 99 bps is created.

Table 3.1 Sequences used as sgRNA to knock out *FLC* exon 1 in *Noccaea caerulescens*.

Sticky end overhangs that are complementary to sticky overhangs in the recipient vector in a Golden Gateway reaction are underlined.

sgRNA primer name	Sequence (5' to 3')
sgRNA_NcFLC1_fw	ATTGACCTTCTCCAAACGACGCAA
sgRNA_NcFLC1_rev	AAACTTGCGTCGTTTGGAGAAGGT
sgRNA_NcFLC2_fw	ATTGAAGCTCTACAGCTTCTCCTC
sgRNA_NcFLC2_rev	AAACGAGGAGAAGCTGTAGAGCTT

To verify that the sgRNAs binds to *FLC* exon 1 for a large range of *N. caerulescens* accessions, *FLC* exon 1 was amplified for 28 different accessions that form a representative sample of the genotypes present within *N. caerulescens* (Appendix 2). Genomes of various accessions of *N. caerulescens* were sequenced before, however, due to the unavailability of this data the first exon of *FLC* was amplified again. DNA of the 28 accessions was isolated (Appendix 4A). Two primers amplifying *FLC* exon 1 were designed and were first tested on Clough wood (CLW) and GA as a reference (Appendix 4B) to verify that the primers work as intended under the used cycling conditions. Both primer pairs amplified *FLC* exon 1 and primer pair one (Table 2.1) was then successfully used to amplify *FLC* exon 1 for all selected accessions, except for Copenhagen (COP), in a PCR reaction (Fig. 3.1A). The PCR on COP was rerun using primer pair two (Table 2.1) after which *FLC* exon 1 was successfully amplified (Fig. 3.1B). Sanger sequencing results were aligned to the reference genome of GA (Fig. 3.1C). No mismatches were found for the target sequence of sgRNA2, indicating that sgRNA2 is universally applicable for all verified accessions. The amplicon of the Fresse sur Moselle-2 (FSM2) accession was shorter than the other amplicons and shows one mismatch at the 6th base-pair of the sgRNA in the alignment of the targeting sequence of sgRNA1. The mismatch is a synonymous mutation. Based on the representative sample of *N. caerulescens* accessions that was tested the designed sgRNAs will mutate *FLC* in all of these accessions, thus the sgRNAs were cloned into an expression vector for further use.

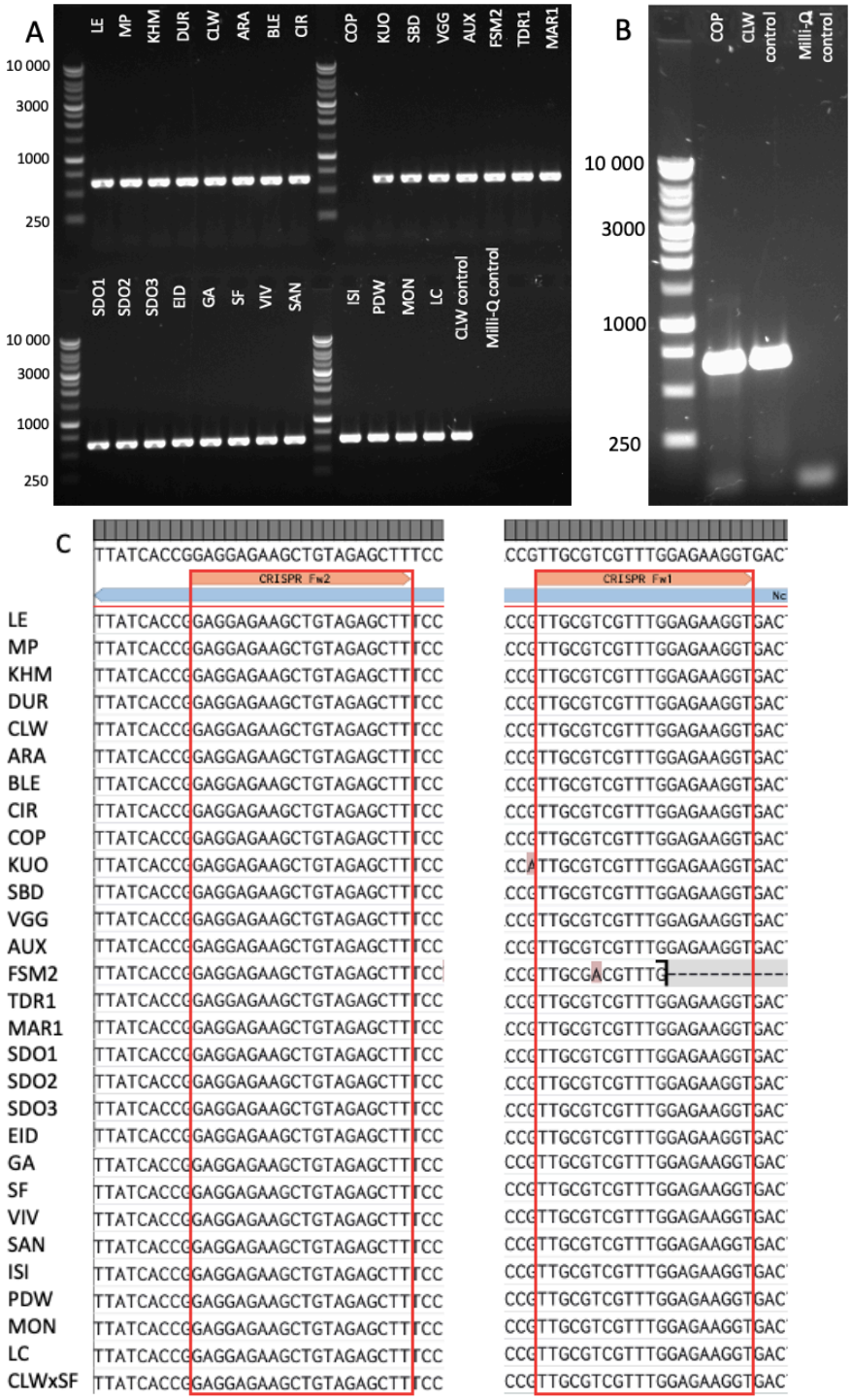

Figure 3.1 Validation experiment of *FLC* exon 1 of 28 diverse *N. caerulescens* accessions.

A: Validation of *FLC* exon 1 PCR on *N. caerulescens* accessions using primer pair 1. An amplicon is visible for all the accessions, except for Copenhagen (COP). CLW was used as a control and milli-Q water was used as a negative control. A 10kb ladder is shown. B: Validation of *FLC* exon 1 PCR on the COP accession using primer pair 2. CLW was used as a positive control and milli-Q water was used as a negative control. A 10kb ladder is shown. C: Alignment of *FLC* exon 1 to the designed sgRNAs. The top row indicates the reference sequence (GA), and the red box outlines the sgRNAs. Mismatches are marked in red. On the left the alignment for sgRNA2 is visible and on the right for sgRNA1. The missing base pairs visible in the Fresse sur Moselle-2 (FSM2) accession do not indicate a deletion, but indicate the end of the amplicon.

Transformation of *Agrobacterium tumefaciens* with the CRISPR construct to knock out *FLC* in *N. caerulescens*

After confirming the applicability of the designed sgRNAs on a representative sample of *N. caerulescens* accessions, the sgRNAs were cloned into an expression vector via Golden Gateway cloning. First, sgRNA1 was cloned into an M1 shuttle vector and sgRNA2 was cloned into an M2E shuttle vector via a digestion-ligation reaction (Fig. 2.2). Initial attempts failed as no colonies grew on the selective agar plates. I hypothesized that the annealing of the sgRNAs had failed, as the insertion of an empty shuttle vector in competent TopTen *E. coli* would lead to cell death due to a *ccdB* gene that was present in the shuttle vector. This *ccdB* gene is cut out and replaced by the sgRNA upon a successful digestion-ligation reaction. Therefore, instead of milli-Q an annealing buffer was added in the sgRNA hybridization reaction. This annealing buffer included Tris to stabilize the pH, EDTA to protect against DNA degradation by chelating divalent cations of nucleases, and NaCl to ensure a stringent hybridization and to provide the necessary ionic strength (Annealing Oligonucleotides Protocol, z.d.). After adding an annealing buffer during sgRNA hybridization, colony formation on the plates was observed.

After plasmid isolation the concentration was measured using a DeNovix DS-11 FX Spectrophotometer/Fluorometer. Measured concentrations were around 2000 ng/µL, which was around 50-fold more than expected. These high DNA concentrations were verified using a Qubit. The Qubit on the other hand showed very low plasmid concentrations of below 10 ng/µL. An ethidium bromide agarose gel electrophoresis did not show any plasmid, indicating that the Qubit showed a more accurate plasmid concentration and was therefore used to measure plasmid concentrations after all future plasmid isolations.

The low concentrations of plasmid after the miniprep further indicated that the miniprep had not successfully isolated the plasmid. The in-house miniprep that was used was redone, but failed to isolate plasmid DNA again. For this reason, the Nucleospin Plasmid EasyPure miniprep kit was used instead, which did successfully isolate the plasmid and showed higher (~100 ng/µL) plasmid concentrations (Appendix 5A).

After the aforementioned alterations, I confirmed that competent TopTen *E. coli* cells were successfully transformed with the shuttle vectors containing the sgRNAs by aligning Sanger sequencing results to the expected shuttle vector DNA sequence (Fig. 3.2A). The validated shuttle vectors were then used in a digestion-ligation reaction to form the final transformation vector (Fig. 2.2). Competent TopTen *E. coli* cells were transformed with the transformation vector. A restriction enzyme digestion reaction was performed to get an indication if the transformation vector isolated from the transformed *E. coli* contained the sgRNAs (Appendix 5B). An additional band was visible for an empty transformation vector, due to the presence of an additional cut site. The digestion reaction showed no additional band for any of the isolated plasmids, indicating the presence of the sgRNA. The plasmid was sequenced at PlasmidSaurus to obtain the full sequence of the plasmid. Both sgRNAs had correctly inserted. Moreover, an insertion in the backbone of 150 bp that was not expected was found (Fig. 3.2B). A BLASTn search on NCBI indicated that the insertion is related to Cas9 (100% query cover, 100% identity and an E-value of $2.7*10^{-2}$) which is to be expected, as the vector backbone includes a CRISPR-Cas9 construct.

Lastly, the transformation vector was inserted into *A. tumefaciens* and verified by transforming *E. coli* with the isolated vector from *A. tumefaciens*. A restriction enzyme digestion showed that the *E. coli,* and therefore the *A. tumefaciens,* contain the transformation vector including sgRNAs (Fig. 3.2C). To conclude, I successfully transformed *A. tumefaciens* with a transformation vector that can knock out *FLC* via a CRISPR-Cas9 system, thereby creating early flowering *N. caerulescens* lines.

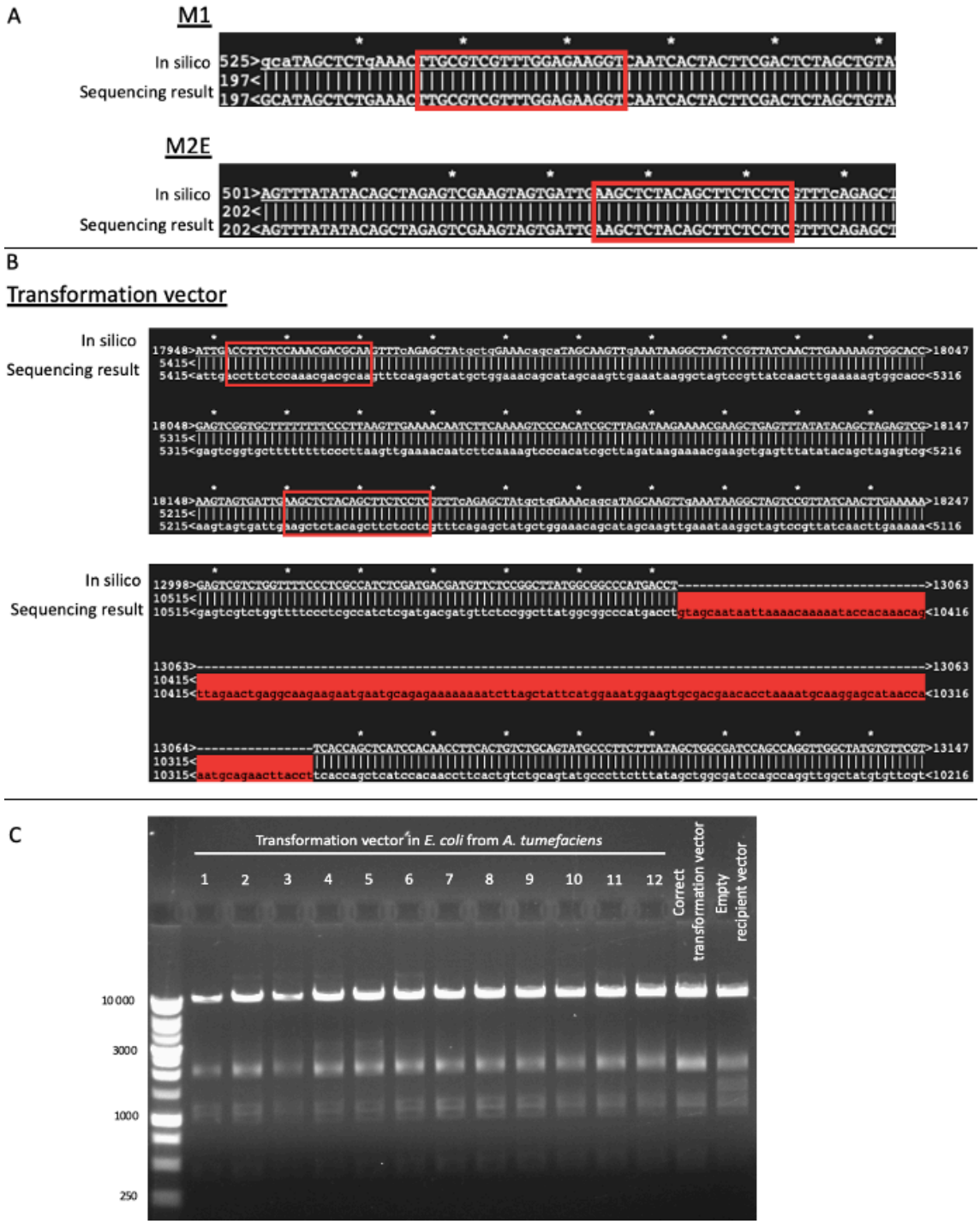

Figure 3.2 Golden Gateway cloning of the *FLC* sgRNAs.

A: Alignment of the expected sequence (top row) to the sequencing results (bottom row) of the M1 and M2E shuttle vector. The sgRNAs are indicated by the red boxes. B: Alignment of the expected sequence (top row) to the sequencing results (bottom row) of the transformation vector. The sgRNAs are indicated by the red boxes. The sequence highlighted in red indicates an insertion in the vector backbone. C: Gel of the digestion of the transformation vector containing both sgRNA inserts. The empty recipient vector and a previously validated transformation vector were used as controls. The plasmid was isolated from *E. coli* that had been transformed using the transformation vector as isolated from transformed *A. tumefaciens*. A 10kb ladder is shown.

3.2 The effect of a *bzip19* mutation on *zinc,* nickel, and cadmium homeostasis in *N. caerulescens*

Introgression of a mutated *flc* may be used as an alternative to the CRISPR construct to generate early flowering *N. caerulescens* lines. In an introgressed early flowering Clough Wood line, *bZIP19* was knocked out to determine the effect of *bzip19* on hyperaccumulation in *N. caerulescens*.

A *bzip19* knockout does not appear to affect Zinc hyperaccumulation in *N. caerulescens*

To determine the effect of a *bzip19* mutation on Zn hyperaccumulation in *N. caerulescens,* a dosing experiment was performed. Mutant plants developed poorly in the Zn dosing experiment due to poor root formation, causing few replicates (n = 4, 2, 5). When roots did not reach the liquid Hoagland, growth was halted, and plants remained the same size throughout the experiment. Because of the low number of replicates and the poor development of the mutant in the first trial, a second trial was run. Plant development of the mutant plants before treatment during the second trial was more similar to the plant development before treatment in the Ni and Cd dosing experiment (Appendix 6A). In the second trial most wildtype plants died before treatment was started, likely due to poor root formation, causing low numbers of replicates for the wildtype in trial two (n = 2, 1, 2). Due to the low number of replicates in both trials no statistical analysis was performed. During the first trial no clear differences in Zn content in the shoot material was found between the *bZIP19* wildtype and the *bzip19* mutant (Fig. 3.3). During the second trial there appears to be less Zn uptake by the *bzip19* mutant under low Zn conditions (2 μM and 20 μM) (Fig. 3.3). Some small plants (<50 mg dry weight) are shown in the figure, that can affect the conclusion drawn. If these plants are excluded the difference between the wildtype and *bzip19* mutant in 2 μM Zn mostly falls away. Taken together the results do not suggest that Zn accumulation in the shoots in *bzip19* is different from *bZIP19* wildtype plants.

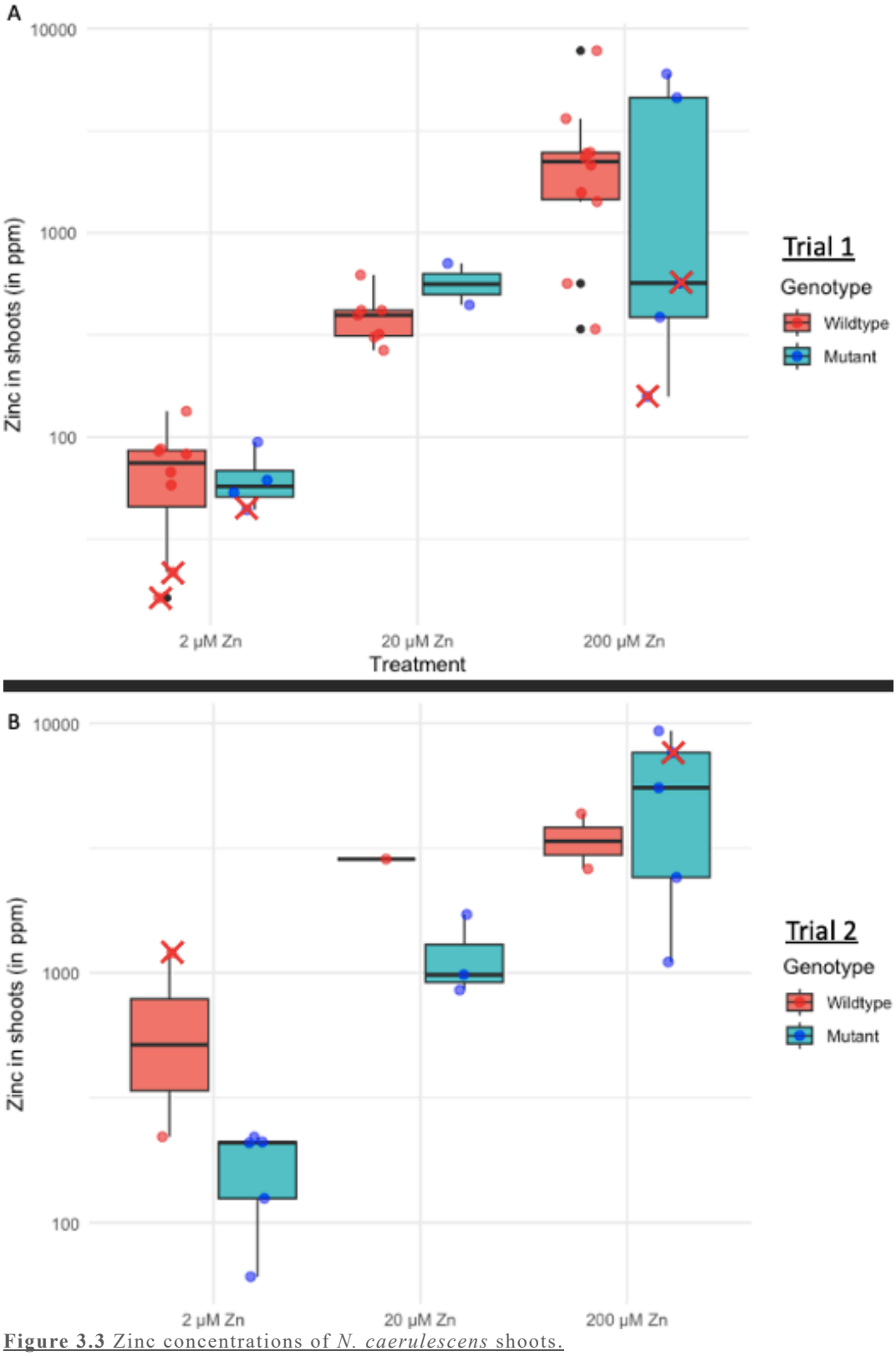

Figure 3.3 Zinc concentrations of *N. caerulescens* shoots.

bZIP19 wildtype *N. caerulescens* are compared to *bzip19* mutants. Concentrations are shown in parts per million on a logarithmic scale. Trial 1(A) and Trial 2 (B) are shown. Individual measurements are shown with red (wildtype *bZIP19*) and blue (mutant *bzip19*) dots. Black dots indicate outliers in the boxplot. Black dots are shown also by its corresponding, coloured dot (blue or red). Red crosses indicate plants that had a dry weight below 50 mg.

Trial 1: 2 µM Zn ($n_{Wildtype}$=8, n_{mutant}=4), 20 µM Zn ($n_{Wildtype}$=7, n_{mutant}=2), and 200 µM Zn ($n_{Wildtype}$=10, n_{mutant}=5).

Trial 2: 2 µM Zn ($n_{Wildtype}$=2, n_{mutant}=5), 20 µM Zn ($n_{Wildtype}$=1, n_{mutant}=3), and 200 µM Zn ($n_{Wildtype}$=2, n_{mutant}=5).

A *bzip19* knockout takes up less Ni in *N. caerulescens*

Ni is similar to Zn and may be taken up via the same pathways (Deng *et al.*, 2019). To determine if the inactivation of *bZIP19* affects Ni uptake, the Ni concentration was measured in shoots and roots. In shoots, less Ni was taken up by the *bzip19* mutant plants compared to the wildtype (p-value = 0.00079 and p-value = 0.00025 for 10 µM and 100 µM Ni respectively) (Fig. 3.4A), and in roots a similar trend can be seen (Fig. 3.4B). Root samples were combined as root samples were mostly too small to be measured using the Z-Spec, leading to smaller sample sizes. Therefore, no statistical tests were performed on the roots. Various other elements were also measured, and Fe is highlighted here. In all three treatments a lower concentration of Fe is observed for the *bzip19* mutant compared to the wildtype (p-value = 0.0029, p-value = 0.0014 and p-value = 0.012 for Control, 10 µM and 100 µM Ni respectively) (Fig. 3.4C). Furthermore, in the roots a trend showing more Fe uptake under higher Ni conditions can be observed. Higher concentrations of Ni result in a lower shoot biomass in the bZIP19 wildtype (p-value = 0.03 between the control and 100 µM Ni), but not in the *bzip19* mutant (p-value = 0.98 between the control and 100 µM Ni) (Appendix 6B).

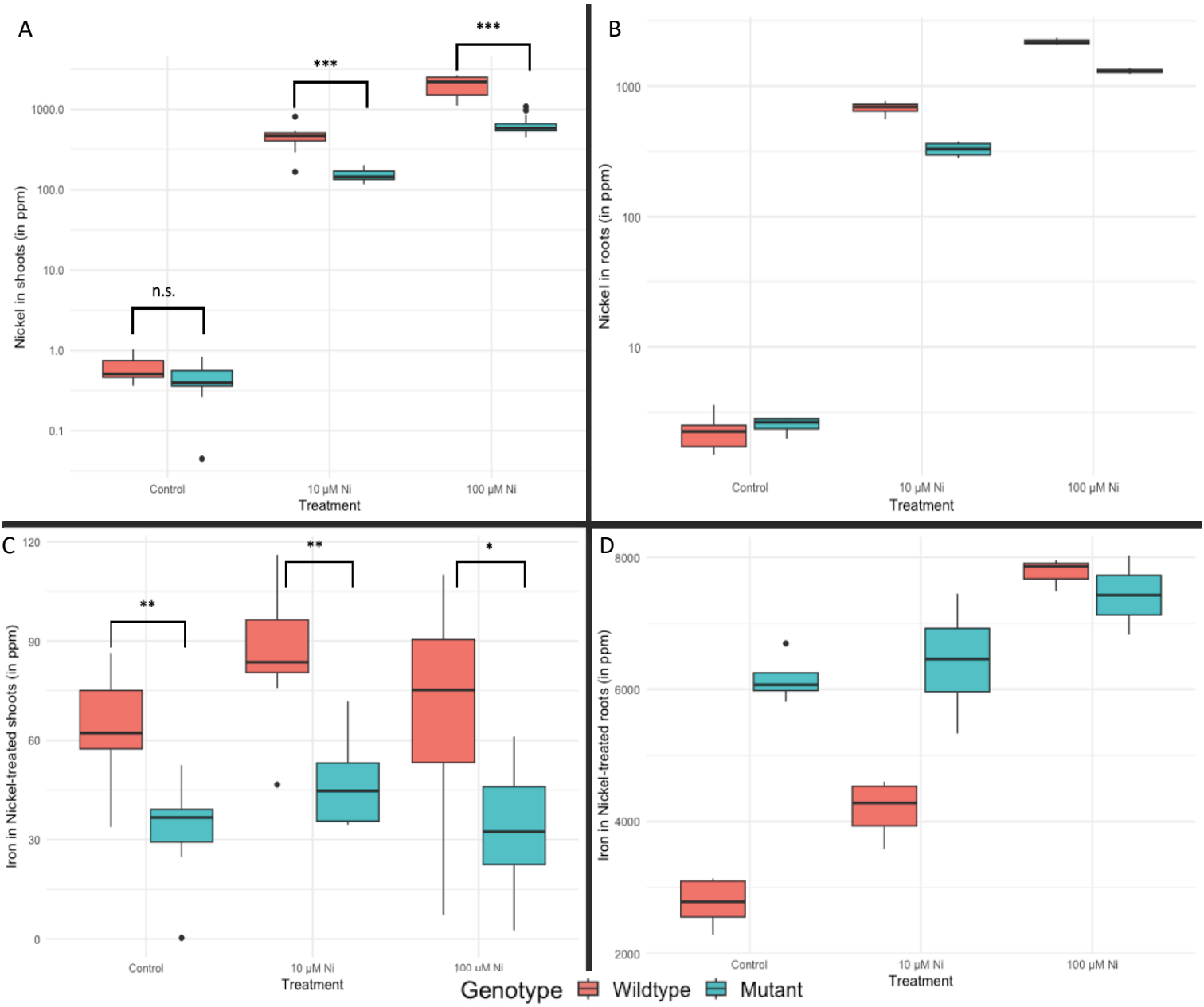

Figure 3.4 Nickel and iron concentrations of Ni-treated *N. caerulescens*.

bZIP19 wildtype *N. caerulescens* (red) are compared to *bzip19* mutants (blue). Concentrations are shown in parts per million for the Control ($n_{Wildtype}$=9, n_{mutant}=10), 10 µM Ni ($n_{Wildtype}$=8, n_{mutant}=12), and 100 µM Ni treatments ($n_{Wildtype}$=8, n_{mutant}=12). Root samples are pooled (Control: $n_{Wildtype}$=7, n_{mutant}=4; Ni 10 µM: $n_{Wildtype}$=4, n_{mutant}=4; Ni 100 µM: $n_{Wildtype}$=3, n_{mutant}=2).

A) Nickel concentrations in shoots are shown with a logarithmic scale (n.s. = not significant ($\alpha = 0.05$), *** = p-value<0.001). B) Ni concentrations in roots with a logarithmic scale. C) Fe concentrations in Ni-treated shoots (* = p-value <0.05, ** = p-value < 0.01). D) Fe concentrations in Ni-treated roots.

A *bzip19* knockout takes up less Cd in high Cd conditions in *N. caerulescens*

Like Ni, Cd can also be taken up via the Zn uptake pathways. To determine the effect of a *bzip19* knock out on the uptake of Cd by *N. caerulescens*, the metal concentrations in the shoots were measured via ICP-AES. Similar levels of Zn and Fe were found in both an ICP-AES measurement and a Z-Spec measurement (Appendix 7), indicating that the ICP-AES measurement was successful and gives a correct indication of metal concentrations. Results

for the control samples, without any added Cd, have not come in yet and are therefore not shown. Under a lower treatment of 2 µM Cd no difference is observed between *bZIP19* wildtype and *bzip19* mutant plants (p-value = 0.89). Under a higher treatment of 20 µM Cd the *bZIP19* wildtype takes up significantly more Cd than the *bzip19* mutant (p-value = 0.0082) (Fig. 3.5). Higher concentrations of Cd cause lower biomass in both the bZIP19 wildtype (p-value = 0.003 between the control and 20 µM Cd) and *bzip19* mutant (p-value = 0.016 between the control and 20 µM Cd) (Appendix 6C).

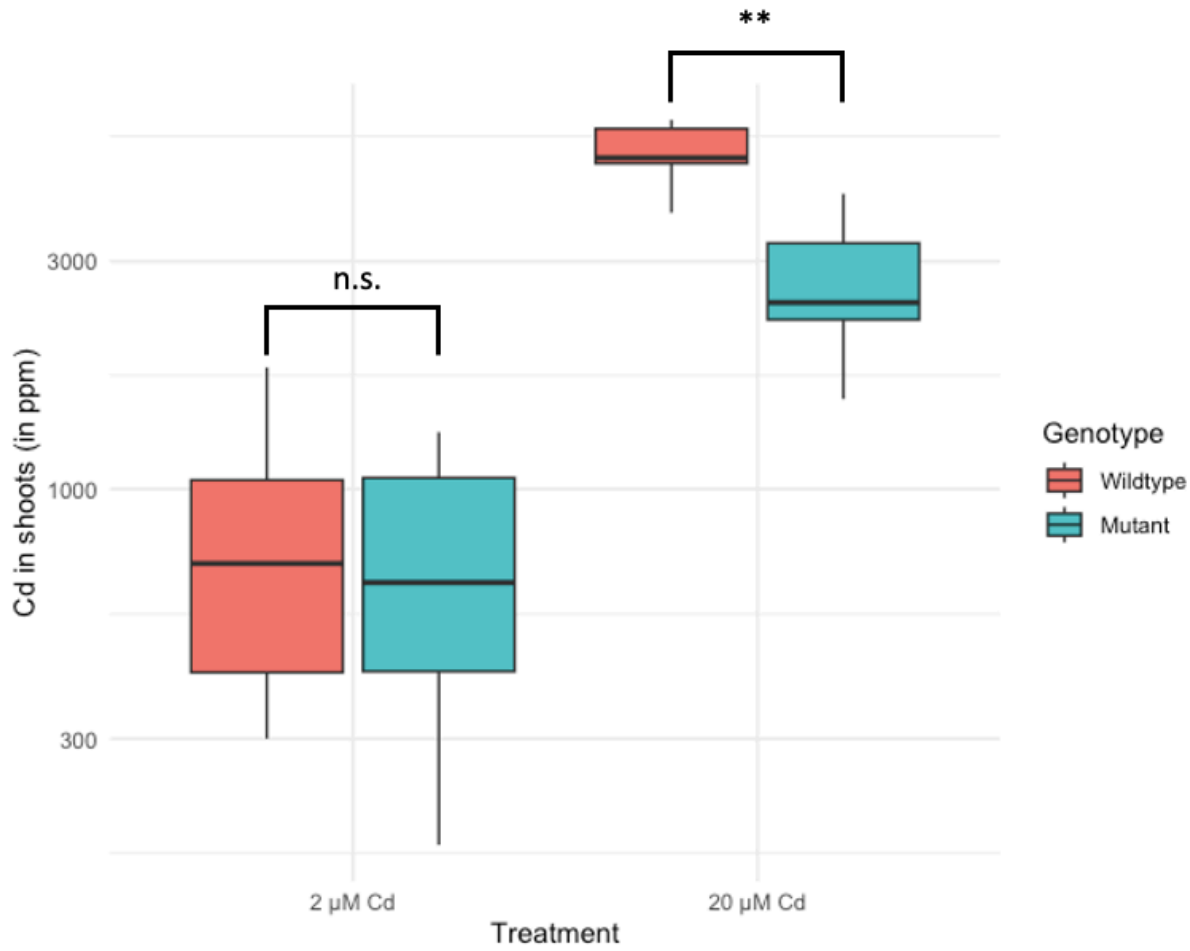

Figure 3.5 Cadmium concentrations in Cd-treated *Noccaea caerulescens.*

Cd content in *bZIP19* wildtype *N. caerulescens* shoots compared to *bzip19* mutants in parts per million in shoots for the 2 µM Cd ($n_{Wildtype}$=8, n_{mutant}=9), and 20 µM Cd treatment (n=6). n.s. = not significant (α = 0.05), ** = p-value<0.01

3.3 Successful transformation of *N. caerulescens* with a CRISPR-Cas9 construct targeting the *ZSM* of *bZIP19*

Instead of removing *bZIP19* via a knockout, the *ZSM* of *bZIP19* can be knocked out, to create a bZIP19 that is hypothesized to be insensitive to Zn and will therefore be constitutively active. *A. tumefaciens* containing a CRISPR construct targeting the *ZSM* of *bZIP19* was previously generated (Lin, 2023; Vijverberg, 2022). The *ZSM*-targeting construct was isolated from *A. tumefaciens* to confirm the sequence. The isolate was transformed into competent TopTen *E. coli* and plated on selective medium with 50 µg/mL Spectinomycin. The verification of the *ZSM*-targeting construct was run in parallel to the generation of the shuttle vector and therefore ran into similar issues with using the DeNovix DS-11 FX Spectrophotometer/Fluorometer to measure DNA concentration and the in-houseminiprep kit (See "Transformation of *Agrobacterium tumefaciens* with the CRISPR construct to knock out

FLC in *N. caerulescens*"). Therefore, the Qubit and the Nucleospin Plasmid EasyPure miniprep kit were used thereafter. Moreover, after continued false positives (colonies without the construct) were isolated, I hypothesized that 50 µg/mL Spectinomycin was too low and increased the selective pressure by doubling the antibiotic concentration. Only colonies containing the construct were found on the higher selective plates. The construct was successfully isolated, based on 1% agarose, ethidium bromide gels, and the construct was sent to PlasmidSaurus for sequencing. Unfortunately, sequencing was unsuccessful, due to an unknown problem. No sequence data was returned by PlasmidSaurus. The original *E. coli* stock containing the *ZSM*-targeting construct that was used to transform *A. tumefaciens* was then used to isolate the construct for sequencing at PlasmidSaurus. The ZSM-targeting construct was successfully sequenced and showed the same insertion in the backbone as the expression vector used for the *FLC* sgRNAs (See "Transformation of *Agrobacterium tumefaciens* with the CRISPR construct to knock out *FLC* in *N. caerulescens*"). The verification of *A. tumefaciens* was not pursued further after the successful sequencing of the *E. coli* stock due to time constraints. The construct in *A. tumefaciens* was assumed to be the same as in the *E. coli* stock.

The *A. tumefaciens* with CRISPR-Cas9 construct targeting the *ZSM* of *bZIP19* was successfully used to transform *N. caerulescens* via floral dipping. A FAST (Fluorescence-Activating and Absorption-Shifting Tag) marker with a red fluorescent protein was present in the construct that was used in the transformation, to allow for selection of transformed seeds (Fig. 3.6). Different methods of transformation were used in an attempt to improve transformation efficiency, namely 0.02% or 0.05% Silwet L-77 and the gentle crushing of flower buds during dipping or no crushing during dipping. The transformed *N. caerulescens* have not yet fully been harvested, due to which no analysis on the effect of the different dipping methods can be performed yet. Preliminary results suggest that a combination of 0.02% Silwet L-77 together with the gentle crushing of the flower buds results in the highest efficiency (n=7).

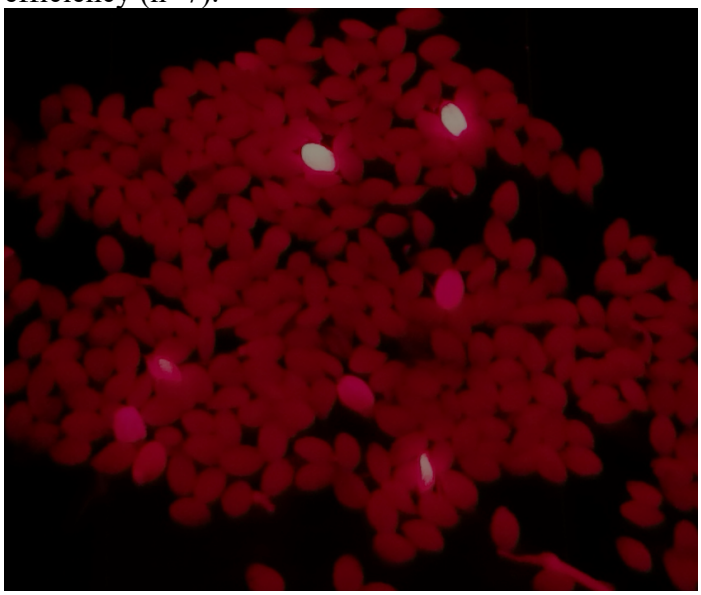

Figure 3.6 Transformed *N. caerulescens* seeds with a CRISPR-Cas9 construct targeting the *ZSM* of *bZIP19.*

Seeds harvested from *N. caerulescens* that was transformed via *A. tumefaciens*-mediated floral dipping are shown. Transformed seeds are bright red to white.

4. Discussion

Hyperaccumulating plants can give insights into genetic pathways that can be targeted for biofortification of foods to mitigate micronutrient deficiency of for example Zn, and can furthermore aid in remediating polluted soil, perhaps even with the option of phytoextraction of more precious elements, like Ni and Cd. *Noccaea caerulescens* serves as an interesting model for hyperaccumulation, due to differences in hyperaccumulation and hypertolerance properties between accessions, allowing comparisons between similar genetic backgrounds (Halimaa *et al.*, 2014). Furthermore, *N. caerulescens* can be genetically altered via *A. tumefaciens*-mediated floral dipping (Yamjabok *et al.*, 2024). One of the current limitations decreasing the efficiency of genetic studies, the long vernalization time and therefore long generation time of *N. caerulescens*, was addressed here. Moreover, the effect of *bzip19* on the levels of Zn, Ni and Cd hyperaccumulated was characterized.

4.1 Creation of a CRISPR-Cas9 construct targeting *FLC* in *N. caerulescens*

FLC plays a central role in regulating flowering time in various plant species by acting as a floral repressor. The function of *FLC* is well-characterized (Gramzow *et al.*, 2023) and involves a highly conserved MADS-box domain of 56 bp with an N-terminal DNA-binding domain that is crucial for *FLC* functioning (Surabhi & Badajena, 2020; Zhang *et al.*, 2024). I successfully transformed *A. tumefaciens* with a vector containing a CRISPR-Cas9 construct and two sgRNAs targeting *FLC* exon 1 that can be used in a wide range of *N. caerulescens* accessions. The versatile applicability of the designed CRISPR construct allows the generation of early flowering lines with various genetic backgrounds.

Though the Golden Gateway protocol used is far advanced and generally efficient, a few areas for improvement are mentioned here. To enhance efficiency of the Golden Gateway cloning in the future, an annealing buffer can be used that may enhance oligonucleotide annealing by providing a stable environment. Moreover, DNA concentrations measured with the DeNovix DS-11 FX Spectrophotometer/Fluorometer should be compared to concentrations measured with the Qubit to see if the concentrations match. If not, I would recommend using the Qubit to measure plasmid concentrations. Lastly, as the Nucleospin Plasmid EasyPure miniprep kit ensued more stable results than the in-house miniprep kit, I suggest using the Nucleospin Plasmid EasyPure miniprep kit. To conclude, I suggest using an annealing buffer during oligonucleotide annealing, using the Qubit to measure the DNA concentration and using the Nucleospin Plasmid EasyPure miniprep kit to isolate the plasmid.

The transformation vector backbone used showed an additional, unexpected insertion. The vector backbone includes a CRIPR-Cas9 construct, and the insertion is likely related to Cas9 (Sagawa *et al.*, 2024). Moreover, the same insert was found in the ZSM construct that was successfully used to transform *N. caerulescens*. The successful application of a construct with this vector backbone, means there is no indication that the insertion will lead to a different functioning of the vector than expected. The sequence of the transformation vector is slightly different than the sequence that was used in the alignment. Therefore, the sequence as used for aligning should be altered, as it is incorrect.

The designed sgRNAs target exon 1 encoding the MADS-box domain, that is crucial for *FLC* function. Non-homologous end joining, the most prominent DNA repair mechanism in plants, is error-prone, often resulting in insertions or deletions (Merker *et al.*, 2024; Puchta, 2005). When CRISPR-Cas9 introduces double-stranded breaks, three potential mutagenic outcomes can be caused by non-homologous end joining. Firstly, improper repair after cleavage at one of the two target sites may lead to an insertion or deletion that can cause a frameshift or premature stop codon, disrupting *FLC* functionality. Secondly, if both sgRNAs induce breaks and the DNA is ligated directly at the site of the cleavage, a 99 bp deletion occurs. This results in the removal of 33 amino acids, likely disrupting the functioning of the

MADS-box and thereby disrupting *FLC* function. Even if the deletion of the 99 bp leaves a (partly) functional *FLC*, screening the population for insertions or deletions that are not a multiple of three can help identify disruptive mutations. Thirdly, repair by non-homologous end joining after cleavage by both sgRNAs may introduce insertions or deletions of varying sizes. Insertions or deletions that are not a multiple of three, are likely to cause frameshifts, or perhaps even premature stop codons, severely disrupting gene function. Based on the possible mutagenic outcomes, the crucial role of the MADS-box N-terminus and the established phenotype of *flc* mutants, I hypothesize that knocking out *FLC* by using the designed CRISPR construct in *N. caerulescens* will lead to early flowering lines without large unwanted pleiotropic effects. Verifying the functioning of the construct by sequencing and phenotypic analysis is essential to confirm the successful disruption of *FLC* and associated desired early flowering phenotype.

Applicability of *FLC*-targeting CRISPR-Cas9 construct in *N. caerulescens*

Within the tested set of *N. caerulescens* accessions, Fresse sur Moselle-2 (FSM2) showed a shorter amplicon compared to other accessions and a mutation in the sgRNA1 target area. The mutation is a synonymous mutation, indicating that the flowering time would likely be unaffected by the base pair alteration. To my knowledge, there is no data available on the flowering time of FSM2. CRISPR-Cas9 is known to tolerate some mismatches in the sgRNA sequence, but mismatches in base pair four to seven mostly abolish activity (Zheng *et al.*, 2017). sgRNA1 is therefore likely non-functional in FSM2, due to the mutation at bp 6. However, sgRNA2 can still target *FLC,* creating a knockout.

To date, only three *N. caerulescens* accessions (Clough Wood, Le Blémard, Saint Baudille) have been successfully transformed (Yamjabok *et al.*, 2024). The accession Cira has more rigid peduncles that are prone to breakage during the handling of floral dipping, making it harder to transform (Yamjabok *et al.*, 2024). The transformation of the accession Werschmatt was also unsuccessful. The unsuccessful transformation of Werschmatt is hypothesized to be caused by a lower susceptibility to *A. tumefaciens* infections (Yamjabok *et al.*, 2024). These examples highlight the difficulties that persist in transforming *N. caerulescens* and how the genotype may affect the transformation efficiency.

Moreover, transformation efficiencies in *N. caerulescens* are relatively low 0.28%-0.6% (Peer *et al.*, 2006; Yamjabok *et al.*, 2024), compared to ~2.28% in *A. thaliana* (Ghedira *et al.*, 2013). An improved protocol for transformation in *N. caerulescens* is therefore desirable. A first attempt at increasing the efficiency was performed here, by using 0.02% and 0.05% Silwet L-77 and by dipping normally or by gently crushing flower buds during dipping. The gentle crushing of flower buds induces wounds, that allow easier penetration by *A. tumefaciens* (Jeong *et al.*, 2024). Preliminary results suggest that 0.02% of Silwet L-77 and wounding of flower buds gives the highest transformation efficiency. Due to the delicate nature of the inflorescence of at least some of the accessions, the *A. tumefaciens* may be pipetted on the flower buds and gentle crushing may be applied without bending the peduncles. A wider range of Silwet L-77 concentrations between 0.01% and 0.05% can also be examined to find an optimal concentration, since so far only 0.02%, 0.05% and 0.1% have been tested in *N. caerulescens* (Clough & Bent, 1998; Yamjabok *et al.*, 2024).

Given the variable success rate of transformation among *N. caerulescens* accessions, alternative methods of creating early flowering lines may be used. *FLC* was successfully mutated via ethyl methanesulfonate mutagenesis (Wang *et al.*, 2022) and via fast neutron mutagenesis (Lochlainn *et al.*, 2010). Moreover, *flc* can be introgressed into different backgrounds (Yamjabok *et al.*, 2024). To minimize the effect of genetic backgrounds, crosses can be made between accessions belonging to the same subgroup within *N. caerulescens* (Fig. 2.1). Furthermore, speed breeding can be used to generate early flowering lines for accessions that remain notorious to transform. Growing the plants under controlled, altered

conditions may accelerate their life cycle (Ćeran *et al.*, 2024) and may be an interesting avenue to explore for *N. caerulescens*. For example, growing the plants under 4 °C accelerates flowering (De Almeida Guimarães *et al*., 2013). Ghosh *et al.* (2018) have provided a detailed protocol for speed breeding for various Brassica species, that could be tested and troubleshooted in *N. caerulescens.* Speed breeding is, however, a vast concept and requires a more in-depth search than provided in this thesis. These alternative approaches may complement a CRISPR-Cas9 based approach, especially in accessions that are more challenging to transform.

4.2 The effect of bZIP19 on Zn, Ni and Cd hyperaccumulation in *N. caerulescens*

A Clough Wood with an introgressed *flc* from Saint Felix de Pallières was transformed with *A. tumefaciens* to create *bzip19* plants to study the effect of the bZIP19 transcription factor on Zn, Ni and Cd hyperaccumulation. In this study, I aimed to determine the effect of a *bzip19* mutation on Zn, Ni and Cd homeostasis in *N. caerulescens*, where I expected less uptake of all three elements in *bzip19* plants. Firstly, though a lot of variation was observed in the Zn experiment, the data so far do not suggest an altered accumulation of Zn in *bzip19* shoots compared to bZIP19 shoots. Secondly, there is less uptake of Ni by *bzip19* shoots, and a similar trend was observed for *bzip19* roots. Lastly, there is less accumulation of Cd by *bzip19* shoots under higher Cd concentrations.

Drawbacks of and recommendations for the dosing experiments

The main drawback of the Zn dosing experiment was the unpredictability of the development of the plants throughout the experiment. Plants that were used for the Cd and Ni experiment had developed well and were well rooted before the start of the treatments. During trial one in the Zn experiment only the wildtype developed in a similar way as in the Ni and Cd experiment. The mutant in the first Zn trial developed poorly, often not forming roots and halting growth prematurely. Plants would, for example stop growing and developing after the formation of the first set of true leaves. During the second Zn trial, *bzip19* plant development was more similar to the development observed in the Ni and Cd experiment with proper rooting and continued growth. However, the majority of wildtype *bZIP19* plants died soon after germination. Poor rooting might be the cause behind the high mortality rate. The stiffness of the half strength Hoagland gelrite is likely an important factor in the variability. Though for all experiments the protocol was followed exactly, there was a lot of variation. The temperature at which the half strength Hoagland gelrite is pipetted into the bottom-cut PCR tubes and the time the tubes are left to dry might influence the stiffness of the gelrite and should thus be standardized. Alternatively, sowing three seeds per tube would induce root competition, which will induce deeper roots (Fleishman *et al.*, 2019). As soon as the roots reach the liquid half strength Hoagland solution they can develop more freely. The best performing plant can be kept, and the competitors can be taken out. However, sowing three seeds would include a new variable, as the germination of all three seeds might be different for the various tubes giving different levels of competition. To conclude, to produce more stable results, the temperature and drying time of the half strength Hoagland gelrite should be optimized to create a standardized protocol.

A few other factors may have influenced the observed results. Firstly, some of the plants had started flowering before the scheduled harvest date. Considering that there is a possibility of the floral transition influencing element uptake and distribution in plants (Küpper & Kochian, 2009; Nakanishi, 2021), the harvest date was moved up to minimize these effects. In future experiments the dosing may be started at a younger age to allow for a longer exposure to the given treatments and plants should be harvested at the first sign of flowering. Secondly, during the Ni and Cd experiment an error was discovered in the pipette that had been used to make the half strength Hoagland. The pipette had a percentage error of 28%, resulting in it taking up 28% less liquid than intended. It is unclear at what time this

error in the pipette arose and how the error affected the Hoagland solution that was used in the experiments. There is a possibility that plants received less nutrients than they should according to the recipe. The concentration of Ni and Cd were unaffected, as they were added using a different pipette and all plants were affected in the same way as the same batch of Hoagland was used for all plants. Lastly, during the Ni and Cd experiments, mites were observed on the pots. Throughout the experiment no mites were ever observed on the plants themselves, and the assumption is that they were fungivorous mites. Fungivorous mites would not eat the plants and therefore I do not expect large effects of the presence of mites in the experiment.

To further improve the dosing experiment protocol, I would recommend refreshing the growth media twice every week from the moment plants are transferred to hydroponics, to prevent any of the elements in the media from depleting. There were no clear signs that growing media became fully depleted of elements before media were replenished in this experiment. However, as plants grow larger, they do consume more of the medium. Replenishing the medium twice every week would ensure an abundance of all the elements and would therefore ensure that the absolute values measured are not limited by the amount of element present. Moreover, to improve the protocol, I would recommend that the roots are desorbed before drying, to remove any exogenous metals (Nishida *et al.*, 2020). Exogenous metals stuck to roots may be measured in root samples giving the impression of high absolute values, whereas in reality these values may be much lower. In this research, high absolute values of Fe in roots were for example observed, with values reaching over 8000 ppm. Moreover, the root dry weight of the plants was in general too low to measure with the Z-Spec. For this reason, samples of the same genotype grown in the same treatment conditions were combined. Therefore, the sample size became too low to perform statistics. Nevertheless, the measured values of the roots can still indicate present trends, that can be verified in the future.

Differential expression of metal uptake and translocation genes between hyperaccumulators and non-hyperaccumulators

A lot of variation, mainly due to poor root formation and subsequently poor growth, was visible in the Zn experiment. So far, the data suggest that there is little difference between *bzip19* knock out and *bZIP19* wildtype plants. The current hypothesis is that Zn concentrations would be lower in a *bzip19* plant. Within the context of the non-hyperaccumulator *A. thaliana*, bZIP19 is responsible for the Zn deficiency response, upregulating Zn uptake and translocation genes only in low Zn conditions (Assunção *et al.*, 2010; Lilay *et al.*, 2019; Lilay *et al.*, 2021). In the hyperaccumulator *Arabidopsis halleri HEAVY METAL ATPASE 4* (*HMA4*), responsible for translocating Zn from roots to shoots, is highly expressed (Hanikenne *et al.*, 2008). The high expression of *HMA4*, that was also found in *N. caerulescens* (Lochlainn *et al.*, 2011), depletes Zn in roots, causing a constitutive upregulation of bZIP19 target genes due to a continuous Zn deficient state (Hanikenne *et al.*, 2008; Merlot *et al.*, 2020). Silencing *bZIP19* and *bZIP23* did not affect the transcription of *HMA4* (Spielmann *et al.*, 2024), suggesting that *HMA4* is not one of the target genes of bZIP19, and *HMA4* would therefore still be active and highly expressed in a *bzip19 N. caerulescens*. Not all *N. caerulescens* accessions hyperaccumulate Zn and Cd (Halimaa *et al.*, 2014), perhaps due to differences in expression level or copy number of *HMA4*, which may be an interesting avenue to explore in the future. Moreover, (partial) silencing of *bZIP19* and *bZIP23* in *A. halleri* led to a higher accumulation of Zn and Cd, suggesting a backup system to accumulate Zn and Cd is present in *A. halleri* (Spielmann *et al.*, 2024). *IRON REGULATED TRANSPORTER 1* (*IRT1*), an important regulator of Fe uptake, is suggested as an alternative route of uptake of Zn and Cd (Korshunova, 1999; Shanmugam *et al.*, 2013; Spielmann *et al.*, 2024). The presence of a backup system to accumulate Zn and Cd might

explain why no differences were found in the Zn dosing experiment and in the lower Cd concentration. However, under higher Cd concentrations the lack of *bZIP19* did significantly lower the uptake of Cd, suggesting that at least some of the target genes of bZIP19 are responsible for the hyperaccumulation of Cd in *N. caerulescens*.

Lower Ni and Fe uptake in Ni-treated *bzip19 N. caerulescens* shoots

Similar to the Cd dosing experiment, the Ni dosing experiment showed less uptake of Ni in the shoots of the *bzip19* mutants, and a similar trend was observed in the roots. A lowered uptake of Ni by mutant plants indicates that the target genes of the bZIP19 transcription factor are responsible for part of the uptake of Ni by *N. caerulescens*. The uptake of Ni by Zn transporters hypothesized here is in line with a previous hypothesis that stated that Zn transporters are the main transporters for Ni in *N. caerulescens* (Deng *et al.*, 2019). However, the target genes of bZIP19 are not the only genes encoding for transporter proteins involved in the uptake of Ni or Cd, as plants were still able to accumulate Ni and Cd in shoot material. Ni may also be taken up by the Fe pathway (Nishida *et al.*, 2011), therefore possibly affecting Fe homeostasis.

Understanding the effect of Ni on Fe homeostasis may give relevant insights into the broader implications of a *bzip19* knockout, as there is interplay between Zn, Ni, Cd and Fe due to the similarity of these elements (Huang *et al.*, 2024; Korshunova, 1999; Ming et al., 2016; Nishida *et al.*, 2011). In the Ni-treated plants Fe content was consistently lower in *bzip19* shoots compared to bZIP19 shoots, even in the control treatment, suggesting that bZIP19 target genes are partly responsible for Fe translocation in *N. caerulescens*. Moreover, an apparent increase in Fe content in roots was observed primarily in bZIP19 plants under increasing Ni concentrations. The *bzip19* mutant showed a similar trend, though less pronounced due to the higher level of Fe in the control and Ni 10 µM treatments. *Allysum inflatum* also shows increasing levels of Fe in roots under increasing Ni conditions (Ghasemi *et al.*, 2009). However, Fe levels in the shoot decrease under increasing Ni conditions in *Allysum inflatum* (Ghasemi *et al.*, 2009), whereas shoot Fe levels remain constant in *N. caerulescens*. Ni competition with Fe can lead to an Fe-deficient state, inducing the upregulation of the iron deficiency pathway in *A. thaliana* (Lešková *et al.*, 2017), including the iron transporter gene IRT1 (Nishida *et al.*, 2011). Possibly the induction of the Fe deficiency pathway in *N. caerulescens* and the high amount of Fe in the solution (40 µM instead of the 20 µM regularly used) might have diminished the visible effect of Ni on Fe content. Furthermore, an increased effect of Ni competition was expected in *bzip19*, as Fe can be taken up via the Zn pathway and *bzip19* plants cannot upregulate the Zn deficiency pathway. A Ni treatment concentration of 100 µM might activate pathways beyond bZIP19, potentially decreasing the observed effect. Additionally, no clear pattern for Fe could be observed in the Zn-treated *N. caerulescens* plant due to the variable data obtained. As Zn and Fe may also be interchangeably taken up by the same transporters (Lešková *et al.*, 2017), albeit with varying affinities, I expect a *bzip19* mutation to also affect Fe uptake under the various Zn treatments, though this should be verified.

bZIP19 and bZIP23 downstream genes

To elucidate the exact mechanisms responsible for the uptake up Ni and Cd via the Zn pathway in *N. caerulescens* a first step might be to take a closer look at the bZIP19 target genes, starting by determining the effect of the *bzip19* mutation on the expression levels of the target genes. Uptake genes are likely mostly expressed in root material, whereas translocation and sequestration genes may be more highly expressed in shoot material, highlighting the importance of differentiating expression between tissue types (Tufiño *et al.*, 2025). Moreover, the interplay between the elements and the effect, for example of Ni on both the Zn and Fe homeostasis pathway indicate that treatments may also affect expression patterns and should therefore be taken into consideration. After determining the effect of the

bzip19 mutation on the expression level in shoots and roots in the various treatments, the most promising genes can be phenotyped for Ni, Cd, Zn and Fe.

bZIP19 and bZIP23 regulate various downstream genes to upregulate Zn uptake and translocation under Zn deficient conditions. The high-affinity Zn uptake transporters, *ZIP3* and *ZIP5*, are mainly regulated by bZIP19 (Inaba *et al.*,2015). *ZIP3* and *ZIP5* are functionally redundant and thought to regulate the main Zn uptake root, regulating Zn homeostasis in Zn deficient states in *A. thaliana* (Tufiño *et al.*, 2025). The expression level of *ZIP3* and *ZIP5* is therefore, likely lower in *bzip19 N. caerulescens* roots, leading to lower uptake of Zn via that pathway. Another downstream gene induced by bZIP19 and bZIP23, *AtZIP4*, is among the first to be induced, primarily inducing Zn uptake for xylem-mediated transport (Lilay *et al.*, 2019; Lin *et al.*, 2016; Tufiño *et al.*, 2025). An ortholog of *AtZIP4*, *NcZNT1*, was found to be highly expressed in *N. caerulescens* and leads to the hyperaccumulation of Zn and Cd upon introduction in *A. thaliana* (Lin *et al.*, 2016; Pence *et al.*, 2000). Expression of *NcZNT1* may be lower in *bzip19 N. caerulescens*, lowering the initial response to Zn deficiency via this pathway. Furthermore, the Zn transporter, *NICOTIANAMINE SYNTHASE 2* (*NAS2*), is highly expressed in the hyperaccumulators *A. halleri* and *N. caerulescens* compared to non-hyperaccumulators and a direct target of bZIP19 and bZIP23 (Assunção *et al.*, 2010b; Deinlein *et al.*, 2012; Hanikenne *et al.*, 2008). *NAS2* may, together with *HMA4* and *NcZNT1*, efficiently remove Zn from the roots thereby depleting the root of Zn leading to a constitutive Zn deficient state in roots. Determining the effect of the *bzip19* mutation on the expression of the main uptake proteins ZIP3 and ZIP5, and the transporters NAS2 and ZNT1 and determining the effect of those genes on the phenotype may give valuable insights into the regulation behind Zn, Ni and Cd hyperaccumulation in *N. caerulescens*.

Zinc-sensing motif knockout

To further understand the functioning of *bZIP19*, *N. caerulescens* was transformed with a CRISPR construct targeting only the *ZSM* while leaving the rest of *bZIP19* intact. In *A. thaliana* knocking out the *ZSM* of *bZIP19* would lead to a higher Zn concentration, due to a constitutive activation of the target genes by bZIP19. However, due to the high expression of *HMA4, ZNT1* and *NAS2* that translocate Zn from roots to shoots (Assunção *et al.*, 2010b; Deinlein *et al.*, 2012; Hanikenne *et al.*, 2008; Lin *et al.*, 2016; Pence *et al.*, 2000), roots may experience a continuous Zn deficient state regardless of the Zn concentration in the growth medium. Therefore, I hypothesize that the concentration of Zn in *zsm* plants will not differ from *ZSM* wildtype plants when using a hyperaccumulating accession. In non-hyperaccumulating accessions of *N. caerulescens* I expect that *zsm* plants will take up more Zn compared to *ZSM* plants, as the downstream genes of bZIP19 will be upregulated constitutively even in high Zn conditions. Moreover, as Ni and Cd are similar to Zn (Deng *et al.*, 2019; Ming *et al.*, 2016), I expect a similar uptake of Ni and Cd in a *zsm N. caerulescens* hyperaccumulator and more uptake of Ni and Cd in a *zsm N. caerulescens* non-hyperaccumulator. Determining the effect of knocking out the *ZSM* of *bZIP19* in both hyperaccumulating and non-hyperaccumulating accessions of *N. caerulescens* will bring us one step closer to understanding the full functioning of *bZIP19* in *N. caerulescens.*

Lacking bZIP23 in Clough Wood *N. caerulescens* accession

Clough Wood contains only a *bZIP19* and lacks *bZIP23* (Lin, 2022). *bZIP19* and *bZIP23* are partly functionally redundant, but show a different expression pattern, with *bZIP19* mostly active in the roots and *bZIP23* mostly active in the shoots in *A. thaliana* (Lilay *et al.*, 2019). Moreover, *ZIP9* is mostly upregulated by bZIP19, whereas *ZIP12* is mostly upregulated by bZIP23 (Inaba *et al.*, 2015), indicating a partly unique function of both bZIPs. bZIP19 and bZIP23 are moreover suggested to be able to form homodimers (Lilay *et al.*, 2019), suggesting that the functionality of bZIP19 will be maintained even in the absence of bZIP23. bZIP19 is suggested to be important for the response in Zn deficient conditions, whereas

bZIP23 regulates Zn homeostasis (Inaba *et al.*, 2015). In a hyperaccumulator Zn homeostasis may be differently regulated, possibly making bZIP23 redundant leading to the loss of the gene. To further understand the function of bZIP23 a background containing both bZIP19 and bZIP23 can be used. The phenotype of a *bzip23* knockout could be determined and compared to a *bzip19* knockout within the same background. Using the designed FLC-CRISPR construct an early flowering *N. caerulescens* line containing both bZIP19 and bZIP23 can be made.

5. Conclusion

To conclude, this thesis shows the successful construction of a versatile tool that can be used to generate early flowering *N. caerluscens* lines. Moreover, I show that knocking out *bZIP19* causes lower uptake of Ni and Cd in shoots, whereas so far, no effect was found on Zn accumulation. The FLC-CRISPR construct that was designed can now be tested and used to create early flowering lines within *N. caerulescens* lines that show differences in hyperaccumulation to get a deeper understanding on the genetic pathways behind hyperaccumulation in *N. caerulescens*. When the mechanisms responsible for hyperaccumulation are elucidated, these pathways can be exploited to biofortify food mitigating micronutrient deficiencies, to remediate polluted soils, and to phytoextract precious elements.

6. Acknowledgements

I would like to express my sincerest gratitude to René Boesten and Ai Lin for helping me throughout my thesis time and providing a really pleasant working environment. I would like to thank Nick Olivier, Mara Krenn, Chiel van Amstel and Anniek Blok for their willingness to bounce ideas on and their input and conviviality. I would further like to thank Mark Aarts and Antony van der Ent for their suggestions. Moreover, a big thank you to Corrie Hanhart and Nick Olivier for germinating and maintaining the *N. caerulescens* accessions used for DNA isolation in this thesis. Thank you to all the people in the thesis ring and René for providing invaluable feedback. Furthermore, I would like to thank Francisca Reyes-Marquez, Corrie Hanhart, Frank Becker and all other lab technicians for always being happy to help, for a clean lab and for their welcoming and warm attitude. Thank you to the department of Genetics for providing such a friendly and meaningful environment throughout my thesis.

References

- Andreini, C., Banci, L., Bertini, I., & Rosato, A. (2006). Zinc through the Three Domains of Life. *Journal Of Proteome Research*, *5*(11), 3173–3178. https://doi.org/10.1021/pr0603699
- Andreini, C., & Bertini, I. (2012). A bioinformatics view of zinc enzymes. *Journal of Inorganic Biochemistry*, *111*, 150–156. https://doi.org/10.1016/j.jinorgbio.2011.11.020
- *Annealing oligonucleotides protocol*. (z.d.). https://www.sigmaaldrich.com/NL/en/technical-documents/protocol/genomics/pcr/annealing-oligos?srsltid=AfmBOor006na__rFa2Le3UegB9Be4lIWem5BwxnHqAfZbnAZZS-ZZKm1
- Assunção, A. G. L., Herrero, E., Lin, Y., Huettel, B., Talukdar, S., Smaczniak, C., Immink, R. G. H., Van Eldik, M., Fiers, M., Schat, H., & Aarts, M. G. M. (2010a). *Arabidopsis thaliana* transcription factors bZIP19 and bZIP23 regulate the adaptation to zinc deficiency. *Proceedings Of The National Academy Of Sciences*, *107*(22), 10296–10301. https://doi.org/10.1073/pnas.1004788107
- Assunção, A. G., Schat, H., & Aarts, M. G. (2010b). Regulation of the adaptation to zinc deficiency in plants. *Plant Signaling & Behavior*, *5*(12), 1553–1555. https://doi.org/10.4161/psb.5.12.13469
- Bechtold, U., Penfold, C. A., Jenkins, D. J., Legaie, R., Moore, J. D., Lawson, T., Matthews, J. S., Vialet-Chabrand, S. R., Baxter, L., Subramaniam, S., Hickman, R., Florance, H., Sambles, C., Salmon, D. L., Feil, R., Bowden, L., Hill, C., Baker, N. R., Lunn, J. E., . . . Mullineaux, P. M. (2016). Time-Series Transcriptomics Reveals That AGAMOUS-LIKE22 Affects Primary Metabolism and Developmental Processes in Drought-Stressed Arabidopsis. *The Plant Cell*, *28*(2), 345–366. https://doi.org/10.1105/tpc.15.00910
- Bouis, H. E., & Welch, R. M. (2010). Biofortification—A Sustainable Agricultural Strategy for Reducing Micronutrient Malnutrition in the Global South. *Crop Science*, *50*(1). https://doi.org/10.2135/cropsci2009.09.0531
- Castro, P. H., Lilay, G. H., Muñoz-Mérida, A., Schjoerring, J. K., Azevedo, H., & Assunção, A. G. L. (2017). Phylogenetic analysis of F-bZIP transcription factors indicates conservation of the zinc deficiency response across land plants. *Scientific Reports*, *7*(1). https://doi.org/10.1038/s41598-017-03903-6
- Ćeran, M., Miladinović, D., Đorđević, V., Trkulja, D., Radanović, A., Glogovac, S., & Kondić-Špika, A. (2024). Genomics-assisted speed breeding for crop improvement: present and future. *Frontiers in Sustainable Food Systems*, *8*. https://doi.org/10.3389/fsufs.2024.1383302
- Clough, S. J., & Bent, A. F. (1998). Floral dip: a simplified method for Agrobacterium-mediated transformation of *Arabidopsis thaliana*. *The Plant Journal*, *16*(6), 735–743. https://doi.org/10.1046/j.1365-313x.1998.00343.x
- Dang, P., & Li, C. (2021). A mini-review of phytomining. *International Journal Of Environmental Science And Technology*, *19*(12), 12825–12838. https://doi.org/10.1007/s13762-021-03807-z
- De Almeida Guimarães, M., Loureiro, M. E., & Salt, D. E. (2013). Inducing flowering in *Noccaea caerulescens* (J. & C. Presl) F. K. Mey (Brassicaceae), a species having high heavy-metal accumulation. *Ciência Agronômica/Revista Ciência Agronômica*, *44*(4), 834–841. https://doi.org/10.1590/s1806-66902013000400021

- Deinlein, U., Weber, M., Schmidt, H., Rensch, S., Trampczynska, A., Hansen, T. H., Husted, S., Schjoerring, J. K., Talke, I. N., Krämer, U., & Clemens, S. (2012). Elevated Nicotianamine Levels in *Arabidopsis halleri* Roots Play a Key Role in Zinc Hyperaccumulation. *The Plant Cell*, *24*(2), 708–723. https://doi.org/10.1105/tpc.111.095000
- Deng, T., Van Der Ent, A., Tang, Y., Sterckeman, T., Echevarria, G., Morel, J., & Qiu, R. (2017). Nickel hyperaccumulation mechanisms: a review on the current state of knowledge. *Plant And Soil*, *423*(1–2), 1–11. https://doi.org/10.1007/s11104-017-3539-8
- Deng, T., Tang, Y., Sterckeman, T., Echevarria, G., Morel, J., & Qiu, R. (2019). Effects of the interactions between nickel and other trace metals on their accumulation in the hyperaccumulator *Noccaea caerulescens*. *Environmental And Experimental Botany*, *158*, 73–79. https://doi.org/10.1016/j.envexpbot.2018.11.015
- Fadzil, F. N. M., Mohamad, M. A. N., Repin, R., & Harumain, Z. A. S. (2024). Metal uptake and tolerance in hyperaccumulator plants: Advancing phytomining strategies. *Rhizosphere*, *29*, 100836. https://doi.org/10.1016/j.rhisph.2023.100836
- Fleishman, S. M., Eissenstat, D. M., & Centinari, M. (2019). Rootstock vigor shifts aboveground response to groundcover competition in young grapevines. *Plant And Soil*, *440*(1–2), 151–165. https://doi.org/10.1007/s11104-019-04059-0
- Genchi, G., Carocci, A., Lauria, G., Sinicropi, M. S., & Catalano, A. (2020a). Nickel: Human Health and Environmental Toxicology. *International Journal Of Environmental Research And Public Health*, *17*(3), 679. https://doi.org/10.3390/ijerph17030679
- Genchi, G., Sinicropi, M. S., Lauria, G., Carocci, A., & Catalano, A. (2020b). The Effects of Cadmium Toxicity. *International Journal Of Environmental Research And Public Health*, *17*(11), 3782. https://doi.org/10.3390/ijerph17113782
- Ghasemi, R., Ghaderian, S. M., & Krämer, U. (2009). Interference of nickel with copper and iron homeostasis contributes to metal toxicity symptoms in the nickel hyperaccumulator plant *Alyssum inflatum*. *New Phytologist*, *184*(3), 566–580. https://doi.org/10.1111/j.1469-8137.2009.02993.x
- Ghedira, R., De Buck, S., Nolf, J., & Depicker, A. (2013). The Efficiency of *Arabidopsis thaliana* Floral Dip Transformation Is Determined Not Only by the Agrobacterium Strain Used but Also by the Physiology and the Ecotype of the Dipped Plant. *Molecular Plant-Microbe Interactions*, *26*(7), 823–832. https://doi.org/10.1094/mpmi-11-12-0267-r
- Ghosh, S., Watson, A., Gonzalez-Navarro, O. E., Ramirez-Gonzalez, R. H., Yanes, L., Mendoza-Suárez, M., Simmonds, J., Wells, R., Rayner, T., Green, P., Hafeez, A., Hayta, S., Melton, R. E., Steed, A., Sarkar, A., Carter, J., Perkins, L., Lord, J., Tester, M., . . . Hickey, L. T. (2018). Speed breeding in growth chambers and glasshouses for crop breeding and model plant research. *Nature Protocols*, *13*(12), 2944–2963. https://doi.org/10.1038/s41596-018-0072-z
- Gramzow, L., Sharma, R., & Theißen, G. (2023). Evolutionary Dynamics of FLC-like MADS-Box Genes in Brassicaceae. *Plants*, *12*(18), 3281. https://doi.org/10.3390/plants12183281
- Guo, B., Zhang, B., Su, Y., Zhang, D., Wang, Y., Bian, Y., Suo, L., Guo, X., & Bai, H. (2021). Retrieving zinc concentrations in topsoil with reflectance spectroscopy at Opencast Coal Mine sites. *Scientific Reports*, *11*(1), 1–20. https://doi.org/10.1038/s41598-021-99106-1
- Halimaa, P., Blande, D., Aarts, M. G. M., Tuomainen, M., Tervahauta, A., & KÃ¤Renlampi, S. (2014). Comparative transcriptome analysis of the metal

hyperaccumulator *Noccaea caerulescens*. *Frontiers in Plant Science*, *5*. https://doi.org/10.3389/fpls.2014.00213

- Haider, F. U., Liqun, C., Coulter, J. A., Cheema, S. A., Wu, J., Zhang, R., Wenjun, M., & Farooq, M. (2021). Cadmium toxicity in plants: Impacts and remediation strategies. *Ecotoxicology And Environmental Safety*, *211*, 111887. https://doi.org/10.1016/j.ecoenv.2020.111887
- Hanikenne, M., Talke, I. N., Haydon, M. J., Lanz, C., Nolte, A., Motte, P., Kroymann, J., Weigel, D., & Krämer, U. (2008). Evolution of metal hyperaccumulation required cis-regulatory changes and triplication of HMA4. *Nature*, *453*(7193), 391–395. https://doi.org/10.1038/nature06877
- Huang, S., Yamaji, N., & Feng, J., MA. (2024). Metal transport systems in plants. *Annual Review Of Plant Biology*, *75*(1), 1–25. https://doi.org/10.1146/annurev-arplant-062923-021424
- Hussain, A., Jiang, W., Wang, X., Shahid, S., Saba, N., Ahmad, M., Dar, A., Masood, S. U., Imran, M., & Mustafa, A. (2022). Mechanistic Impact of Zinc Deficiency in Human Development. *Frontiers in Nutrition*, *9*. https://doi.org/10.3389/fnut.2022.717064
- Inaba, S., Kurata, R., Kobayashi, M., Yamagishi, Y., Mori, I., Ogata, Y., & Fukao, Y. (2015). Identification of putative target genes of bZIP19, a transcription factor essential for Arabidopsis adaptation to Zn deficiency in roots. *The Plant Journal*, *84*(2), 323–334. https://doi.org/10.1111/tpj.12996
- Jeong, J., Jeon, E., Hwang, M. K., Song, Y. J., & Kim, J. (2024). Development of super-infective ternary vector systems for enhancing the Agrobacterium-mediated plant transformation and genome editing efficiency. *Horticulture Research*, *11*(9). https://doi.org/10.1093/hr/uhae187
- Kaur, H., & Garg, N. (2021). Zinc toxicity in plants: a review. *Planta*, *253*(6). https://doi.org/10.1007/s00425-021-03642-z
- Kaur, H., Srivastava, S., Goyal, N., & Walia, S. (2024). Behavior of zinc in soils and recent advances on strategies for ameliorating zinc phyto-toxicity. *Environmental And Experimental Botany*, *220*. https://doi.org/10.1016/j.envexpbot.2024.105676
- Khan, M. A., & Wen, J. (2020). Evaluation of physicochemical and heavy metals characteristics in surface water under anthropogenic activities using multivariate statistical methods, Garra River, Ganges Basin, India. *Environmental Engineering Research*, *26*(6), 200280–0. https://doi.org/10.4491/eer.2020.280
- Kim, D., & Sung, S. (2014). Genetic and Epigenetic Mechanisms Underlying Vernalization. *The Arabidopsis Book*, *12*, e0171. https://doi.org/10.1199/tab.0171
- Korshunova, Y. O. (1999). The IRT1 protein from *Arabidopsis thaliana* is a metal transporter with a broad substrate range. *Plant Molecular Biology*, *40*(1), 37–44. https://doi.org/10.1023/a:1026438615520
- Kumar, S., Palve, A., Joshi, C., & Srivastava, R. K. (2019). Crop biofortification for iron (Fe), zinc (Zn) and vitamin A with transgenic approaches. *Heliyon*, *5*(6).
- Küpper, H., & Kochian, L. V. (2009). Transcriptional regulation of metal transport genes and mineral nutrition during acclimatization to cadmium and zinc in the Cd/Zn hyperaccumulator, *Thlaspi caerulescens* (Ganges population). *New Phytologist*, *185*(1), 114–129. https://doi.org/10.1111/j.1469-8137.2009.03051.x
- Lee, J. H., Yoo, S. J., Park, S. H., Hwang, I., Lee, J. S., & Ahn, J. H. (2007). Role of SVP in the control of flowering time by ambient temperature in Arabidopsis. *Genes & Development*, *21*(4), 397–402. https://doi.org/10.1101/gad.1518407
- Lešková, A., Giehl, R. F., Hartmann, A., Fargašová, A., & Von Wirén, N. (2017). Heavy Metals Induce Iron Deficiency Responses at Different Hierarchic and

Regulatory Levels. *PLANT PHYSIOLOGY*, *174*(3), 1648–1668. https://doi.org/10.1104/pp.16.01916

- Li, P., Lin, C., Cheng, H., Duan, X., & Lei, K. (2015). Contamination and health risks of soil heavy metals around a lead/zinc smelter in southwestern China. *Ecotoxicology And Environmental Safety*, *113*, 391–399. https://doi.org/10.1016/j.ecoenv.2014.12.025
- Li, X., Zhou, Y., & Zhang, J. (2021). Status and associated human health risk of zinc accumulation in agricultural soils across China. *Process Safety And Environmental Protection*, *146*, 867–876. https://doi.org/10.1016/j.psep.2020.12.017
- Lilay, G. H., Castro, P. H., Campilho, A., & Assunção, A. G. L. (2019). The Arabidopsis bZIP19 and bZIP23 Activity Requires Zinc Deficiency – Insight on Regulation From Complementation Lines. *Frontiers in Plant Science*, *9*. https://doi.org/10.3389/fpls.2018.01955
- Lilay, G. H., Persson, D. P., Castro, P. H., Liao, F., Alexander, R. D., Aarts, M. G. M., & Assunção, A. G. L. (2021). Arabidopsis bZIP19 and bZIP23 act as zinc sensors to control plant zinc status. *Nature Plants*, *7*(2), 137–143. https://doi.org/10.1038/s41477-021-00856-7
- Lin, A. (2023). *Gene-editing of Zn sensing in Zn hyperaccumulator Noccaea caerulescens.* [Master's Thesis, Wageningen University & Research].
- Lin, Y., Hassan, Z., Talukdar, S., Schat, H., & Aarts, M. G. M. (2016). Expression of the ZNT1 Zinc Transporter from the Metal Hyperaccumulator *Noccaea caerulescens* Confers Enhanced Zinc and Cadmium Tolerance and Accumulation to *Arabidopsis thaliana*. *PLoS ONE*, *11*(3), e0149750. https://doi.org/10.1371/journal.pone.0149750
- Lochlainn, S. Ó., Bowen, H. C., Fray, R. G., Hammond, J. P., King, G. J., White, P. J., Graham, N. S., & Broadley, M. R. (2011). Tandem Quadruplication of *HMA4* in the Zinc (Zn) and Cadmium (Cd) Hyperaccumulator *Noccaea caerulescens*. *PLoS ONE*, *6*(3), e17814. https://doi.org/10.1371/journal.pone.0017814
- Lochlainn, S. Ó., Fray, R. G., Hammond, J. P., King, G. J., White, P. J., Young, S. D., & Broadley, M. R. (2010). Generation of nonvernal-obligate, faster-cycling *Noccaea caerulescens* lines through fast neutron mutagenesis. *New Phytologist*, *189*(2), 409–414. https://doi.org/10.1111/j.1469-8137.2010.03554.x
- Merker, L., Feller, L., Dorn, A., & Puchta, H. (2024). Deficiency of both classical and alternative end-joining pathways leads to a synergistic defect in double-strand break repair but not to an increase in homology-dependent gene targeting in Arabidopsis. *The Plant Journal*, *118*(1), 242–254. https://doi.org/10.1111/tpj.16604
- Ming, H., Naidu, R., Sarkar, B., Lamb, D. T., Liu, Y., Megharaj, M., & Sparks, D. (2016). Competitive sorption of cadmium and zinc in contrasting soils. *Geoderma*, *268*, 60–68. https://doi.org/10.1016/j.geoderma.2016.01.021
- Nakanishi, T. M. (2021). Element-Specific Distribution in a Plant. In *Springer eBooks* (pp. 75–107). https://doi.org/10.1007/978-981-33-4992-6_3
- Natasha, N., Shahid, M., Bibi, I., Iqbal, J., Khalid, S., Murtaza, B., Bakhat, H. F., Farooq, A. B. U., Amjad, M., Hammad, H. M., Niazi, N. K., & Arshad, M. (2022). Zinc in soil-plant-human system: A data-analysis review. *The Science Of The Total Environment*, *808*, 152024. https://doi.org/10.1016/j.scitotenv.2021.152024
- Nishida, S., Tanikawa, R., Ishida, S., Yoshida, J., Mizuno, T., Nakanishi, H., & Furuta, N. (2020). Elevated Expression of Vacuolar Nickel Transporter Gene IREG2 Is Associated With Reduced Root-to-Shoot Nickel Translocation in *Noccaea japonica*. *Frontiers in Plant Science*, *11*. https://doi.org/10.3389/fpls.2020.00610

- Nishida, S., Tsuzuki, C., Kato, A., Aisu, A., Yoshida, J., & Mizuno, T. (2011). AtIRT1, the Primary Iron Uptake Transporter in the Root, Mediates Excess Nickel Accumulation in *Arabidopsis thaliana*. *Plant And Cell Physiology*, *52*(8), 1433–1442. https://doi.org/10.1093/pcp/pcr089
- Olivier, N. (2025). Different QTLs for seed and shoot nickel/zinc accumulation in Noccaea caerulescens. [Master's Thesis, Wageningen University & Research].
- Peer, W. A., Mamoudian, M., Lahner, B., Reeves, R. D., Murphy, A. S., & Salt, D. E. (2003). Identifying model metal hyperaccumulating plants: germplasm analysis of 20 Brassicaceae accessions from a wide geographical area. *New Phytologist*, *159*(2), 421–430. https://doi.org/10.1046/j.1469-8137.2003.00822.x
- Peer, W. A., Mahmoudian, M., Freeman, J. L., Lahner, B., Richards, E. L., Reeves, R. D., Murphy, A. S., & Salt, D. E. (2006). Assessment of plants from the Brassicaceae family as genetic models for the study of nickel and zinc hyperaccumulation. *New Phytologist*, *172*(2), 248–260. https://doi.org/10.1111/j.1469-8137.2006.01820.x
- Pence, N. S., Larsen, P. B., Ebbs, S. D., Letham, D. L. D., Lasat, M. M., Garvin, D. F., Eide, D., & Kochian, L. V. (2000). The molecular physiology of heavy metal transport in the Zn/Cd hyperaccumulator *Thlaspi caerulescens*. *Proceedings Of The National Academy Of Sciences*, *97*(9), 4956–4960. https://doi.org/10.1073/pnas.97.9.4956
- Pollard, A. J., Reeves, R. D., & Baker, A. J. (2014). Facultative hyperaccumulation of heavy metals and metalloids. *Plant Science*, *217–218*, 8-17. https://doi.org/10.1016/j.plantsci.2013.11.011
- Puchta, H. (2004). The repair of double-strand breaks in plants: mechanisms and consequences for genome evolution. *Journal Of Experimental Botany*. https://doi.org/10.1093/jxb/eri025
- Reed, K. M., & Bargmann, B. O. R. (2021). Protoplast Regeneration and Its Use in New Plant Breeding Technologies. *Frontiers in Genome Editing*, *3*. https://doi.org/10.3389/fgeed.2021.734951
- Rizwan, M., Usman, K., & Alsafran, M. (2024). Ecological impacts and potential hazards of nickel on soil microbes, plants, and human health. *Chemosphere*, *357*, 142028. https://doi.org/10.1016/j.chemosphere.2024.142028
- Roohani, N., Hurrell, R., Kelishadi, R., & Schulin, R. (2013). Zinc and its importance for human health: An integrative review. *Journal of Research in Medical Sciences: The Official Journal of Isfahan University of Medical Sciences*, *18*(2), 144.
- Sagawa, C. H. D., Thomson, G., Mermaz, B., Vernon, C., Liu, S., Jacob, Y., & Irish, V. F. (2024). An efficient multiplex approach to CRISPR/Cas9 gene editing in citrus. *Plant Methods*, *20*(1). https://doi.org/10.1186/s13007-024-01274-4
- Schoofs, H., Schmit, J., & Rink, L. (2024). Zinc Toxicity: Understanding the Limits. *Molecules*, *29*(13). https://doi.org/10.3390/molecules29133130
- Shanmugam, V., Lo, J., & Yeh, K. (2013). Control of Zn uptake in *Arabidopsis halleri*: a balance between Zn and Fe. *Frontiers in Plant Science*, *4*. https://doi.org/10.3389/fpls.2013.00281
- Sharma, A., Patni, B., Shankhdhar, D., & Shankhdhar, S. C. (2012). Zinc – an indispensable micronutrient. *Physiology And Molecular Biology Of Plants*, *19*(1), 11–20. https://doi.org/10.1007/s12298-012-0139-1
- Stolz, M. L., & McCormick, C. (2020). The bZIP Proteins of Oncogenic Viruses. *Viruses*, *12*(7), 757. https://doi.org/10.3390/v12070757
- Stuttmann, J., Barthel, K., Martin, P., Ordon, J., Erickson, J. L., Herr, R., Ferik, F., Kretschmer, C., Berner, T., Keilwagen, J., Marillonnet, S., & Bonas, U. (2021).

Highly efficient multiplex editing: one-shot generation of 8× *Nicotiana benthamiana* and 12× Arabidopsis mutants. *The Plant Journal*, *106*(1), 8–22. https://doi.org/10.1111/tpj.15197

- Surabhi, G., & Badajena, B. (2020). Recent advances in plant heat stress transcription factors. In *Elsevier eBooks* (pp. 153–200). https://doi.org/10.1016/b978-0-12-819334-1.00010-1
- Tufiño, V. O., Casellas, M. A., Van Duynhoven, A., Flis, P., Salt, D. E., Schat, H., & Aarts, M. G. M. (2025). *Arabidopsis thaliana* Zn transporter genes *ZIP3* and *ZIP5* provide the main Zn uptake route and act redundantly to face Zn deficiency. *The Plant Journal*, *121*(3). https://doi.org/10.1111/tpj.17251
- Vijverberg, S. (2022). *Zinc homeostasis in Noccaea caerulescens: Understanding the role of bZIP19 and bZIP23 in a metal hyperaccumulator species.* [Master's Intership, Wageningen University & Research and Radboud University].
- Wang, Y., Salt, D. E., Koornneef, M., & Aarts, M. G. M. (2022). Construction and analysis of a *Noccaea caerulescens* TILLING population. *BMC Plant Biology*, *22*(1). https://doi.org/10.1186/s12870-022-03739-x
- Wang, Y., Severing, E. I., Koornneef, M., & Aarts, M. G. M. (2020). FLC and SVP Are Key Regulators of Flowering Time in the Biennial/Perennial Species *Noccaea caerulescens*. *Frontiers in Plant Science*, *11*. https://doi.org/10.3389/fpls.2020.582577
- Yamjabok, J., Van der Heijden, L., Koornneef, M., Schat, H., & Aarts, M.G.M. (2024). *An efficient flower dipping transformation method for the metal hyperaccumulator Noccaea caerulescens*. [Doctoral thesis, Wageningen University & Research].
- Zhang, Y., Wang, Y., Ding, Z., Wang, H., Song, L., Jia, S., & Ma, D. (2017). Zinc stress affects ionome and metabolome in tea plants. *Plant Physiology And Biochemistry*, *111*, 318–328. https://doi.org/10.1016/j.plaphy.2016.12.014
- Zhang, Z., Zou, W., Lin, P., Wang, Z., Chen, Y., Yang, X., Zhao, W., Zhang, Y., Wang, D., Que, Y., & Wu, Q. (2024). Evolution and Function of MADS-Box Transcription Factors in Plants. *International Journal Of Molecular Sciences*, *25*(24), 13278. https://doi.org/10.3390/ijms252413278
- Zheng, T., Hou, Y., Zhang, P., Zhang, Z., Xu, Y., Zhang, L., Niu, L., Yang, Y., Liang, D., Yi, F., Peng, W., Feng, W., Yang, Y., Chen, J., Zhu, Y. Y., Zhang, L., & Du, Q. (2017). Profiling single-guide RNA specificity reveals a mismatch sensitive core sequence. *Scientific Reports*, *7*(1). https://doi.org/10.1038/srep40638
- Zou, J., Song, F., Lu, Y., Zhuge, Y., Niu, Y., Lou, Y., Pan, H., Zhang, P., & Pang, L. (2021). Phytoremediation potential of wheat intercropped with different densities of Sedum plumbizincicola in soil contaminated with cadmium and zinc. *Chemosphere*, *276*, 130223. https://doi.org/10.1016/j.chemosphere.2021.130223

Appendix

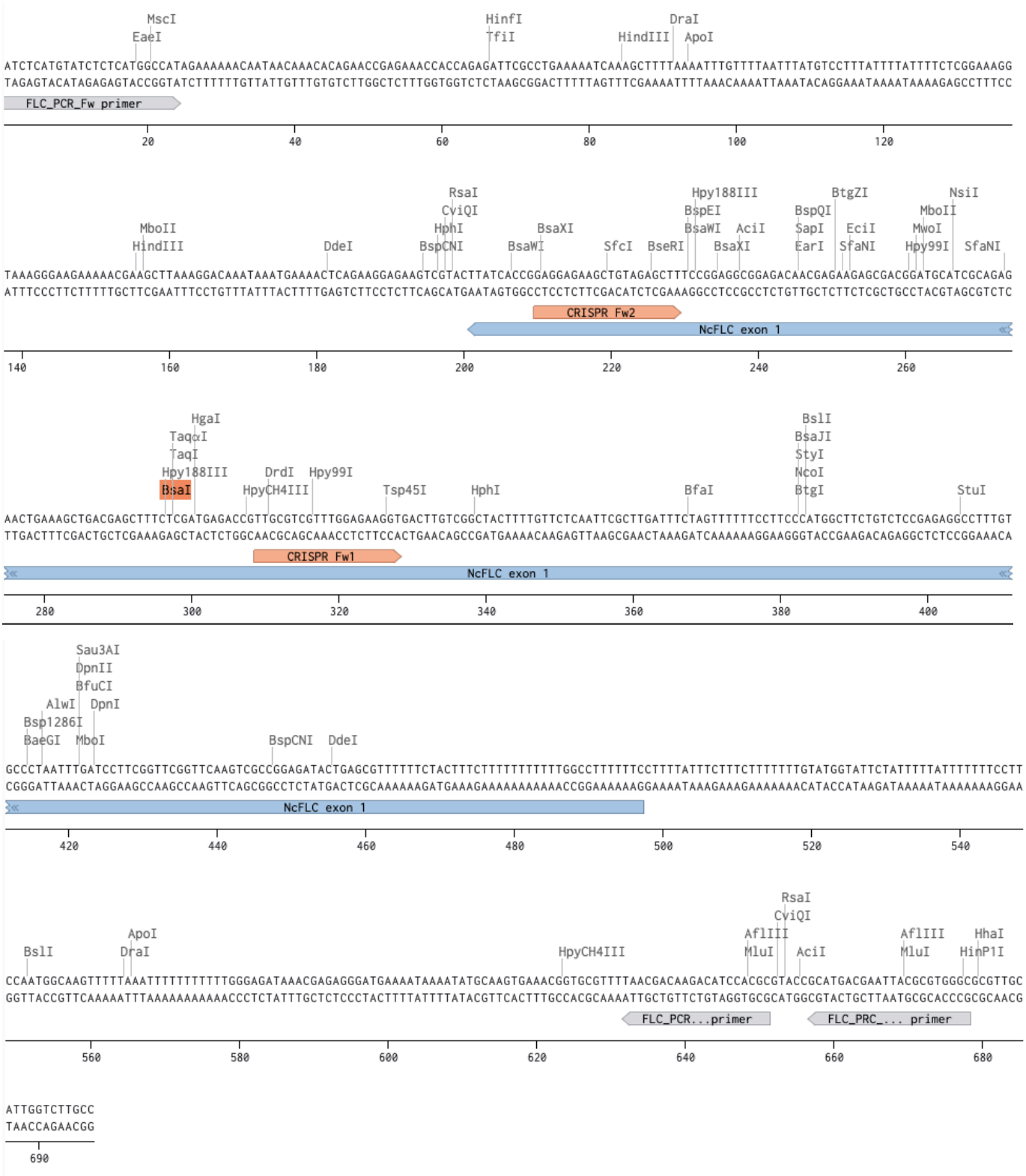

Appendix 1 *FLC* exon 1 Ganges reference DNA sequence.

Reference DNA sequence of the Ganges *N. caerulescens* accession used to design sgRNAs for *FLC* exon 1. The exon sequence is indicated in blue. PCR primer sequences are shown in grey. sgRNA sequences are shown in orange.

Appendix 2 *Noccaea caerulescens* accessions used for *FLC* amplification.

The name of the accession, the abbreviation, the seed code used at Wageningen university, the ecotype and the country of origin are shown. NM = non-metalliferous; ULT = ultramafic; CAL = calmine.

Accession name	Abbreviation	Seed code	Ecotype	Origin
Lellingen	LE	200004	NM	Luxemburg
Monte Prinzera	MP	200005	ULT	Italy
Krušné hory Mountains	KHM	200006	NM	Czech
Durfort	DUR	200007	Cd-CAL	France
Clough Wood, Darley Dale	CLW	200010	Zn-CAL	UK
Puerto de Aralla	ARA	200020	NM	Spain
Le Blémard	BLE	190029	Cd-CAL	France
Cira	CIR	200025	ULT	Spain
Copenhagen	COP	200027	NM	Denmark
Kuopio	KUO	200032	NM	Finland
Saint Baudille	SBD	200033	NM	France
Valle Gargassino	VGG	220014	ULT	Italy
Auxelles	AUX	220015	CAL	France
Fresse sur Moselle-2	FSM2	220041	NM	France
Tête de Ran	TDR1	220030	NM	Switzerland
Col du Marchairuz	MAR1	220076	NM	Switzerland
Spania Dolina	SDO1	220010	CAL	Slovakia
Špania Dolina-2	SDO3	220050	CAL	Slovakia
Špania Dolina-3	SDO3	220057	CAL	Slovakia
Eidian	EID	200030	ULT	Spain
Ganges	GA	200009	Cd-CAL	France
St. Felix de Pallières	SF	200003	Cd-CAL	France
Viviez	VIV	200036	Zn-CAL	France
Sanguinede	SAN	220074	CAL	France
Puerto de San Isidro	ISI	200035	NM	Spain
Puy de Wolf	PDW	200094	ULT	France
Montchamp	MON	220019	NM	France
La Calamine	LC	190003	Zn-CAL	Belgium

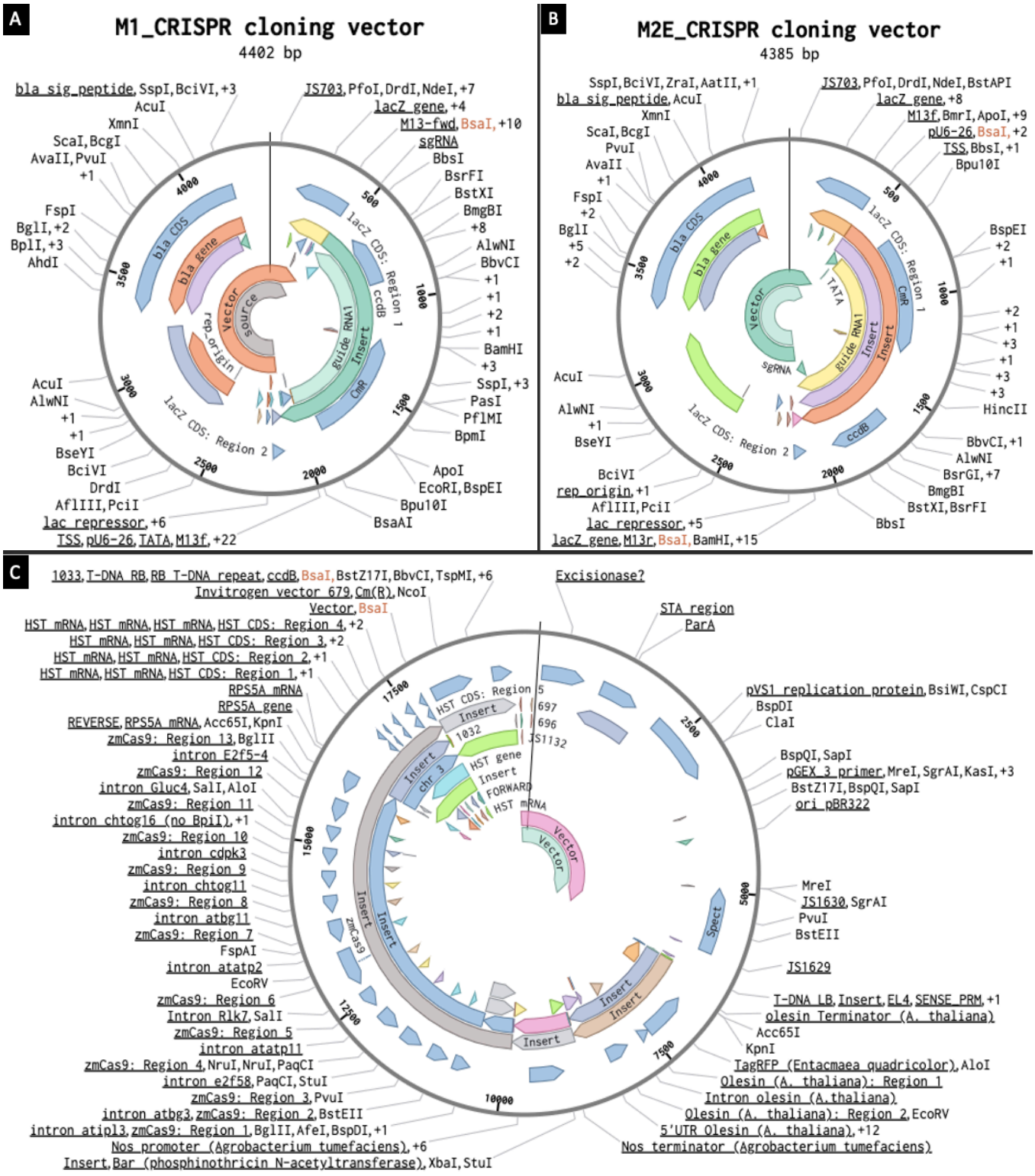

Appendix 3 Shuttle vectors and recipient vectors used in Golden Gateway cloning.

A: Empty M1 shuttle vector. B: Empty M2E shuttle vector. C: Empty recipient vector.

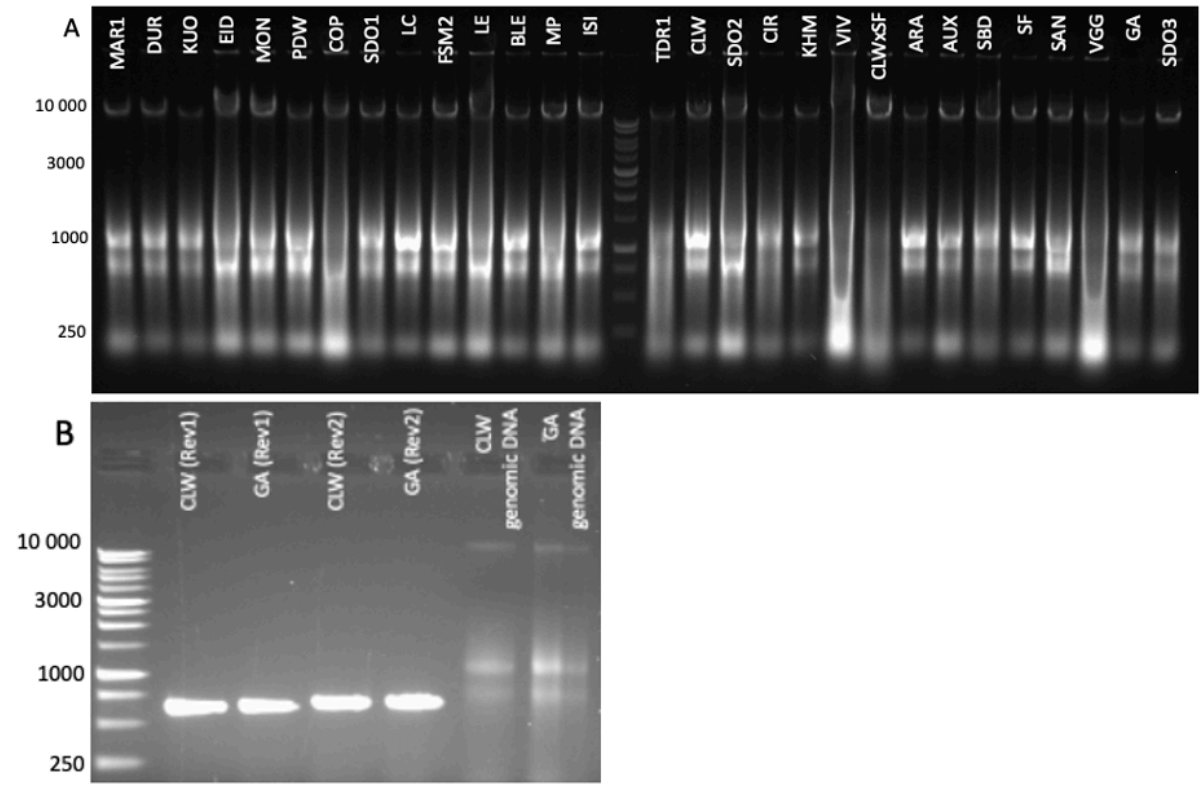

Appendix 4 Validation experiment of *FLC* exon 1 of 28 diverse *N. caerulescens* accessions.

A: DNA isolation of *N. caerulescens* accessions. The line at ~10 000 bp indicates the genomic DNA. A 10kb ladder is shown. B: Validation of *FLC* amplifying primer pair 1 and 2. Clough wood (CLW) and Ganges (GA) were used as reference. A 10kb ladder is shown.

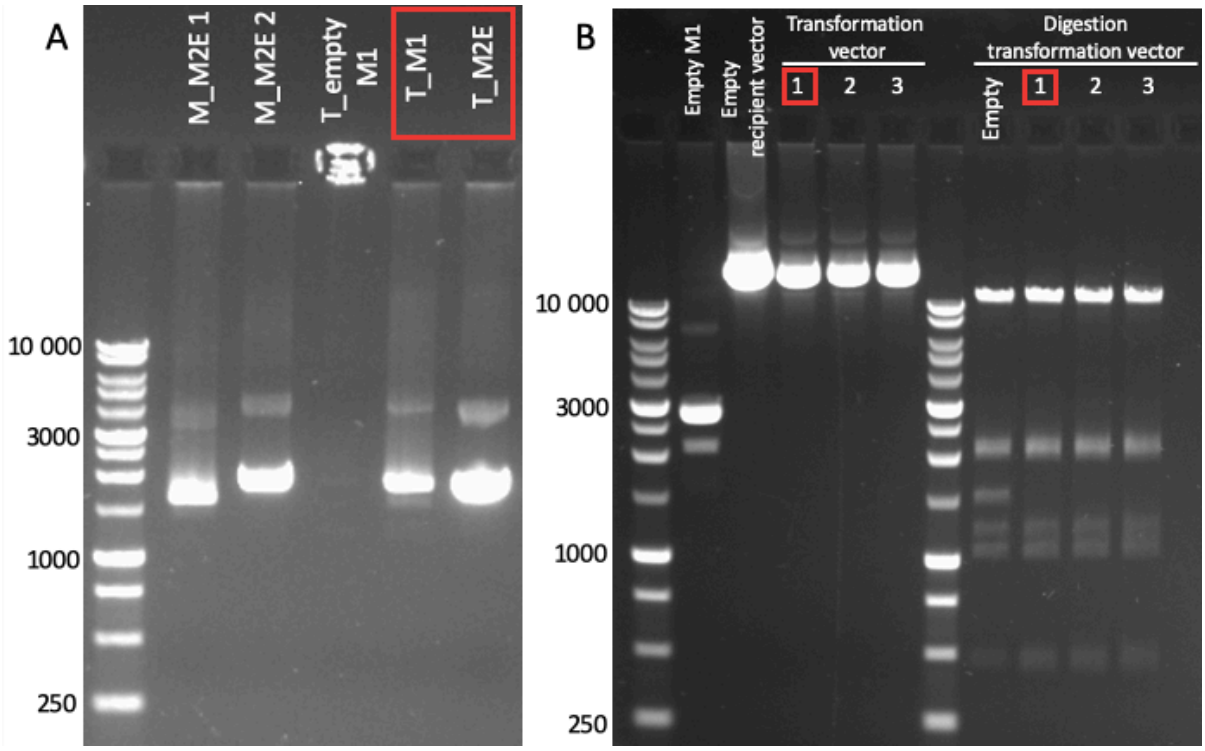

Appendix 5 Gel verifications of the Golden Gateway cloning of the *FLC* sgRNAs.

A: Gel of M1 and M2E plasmid including the sgRNA insert. The red box indicates the two plasmids that were used in future steps. A 10kb ladder is shown. B: Gel of the transformation vector containing both sgRNA inserts. The red box indicates the plasmid that was used in future steps. The empty recipient vector was used as a control. A 10kb ladder is shown.

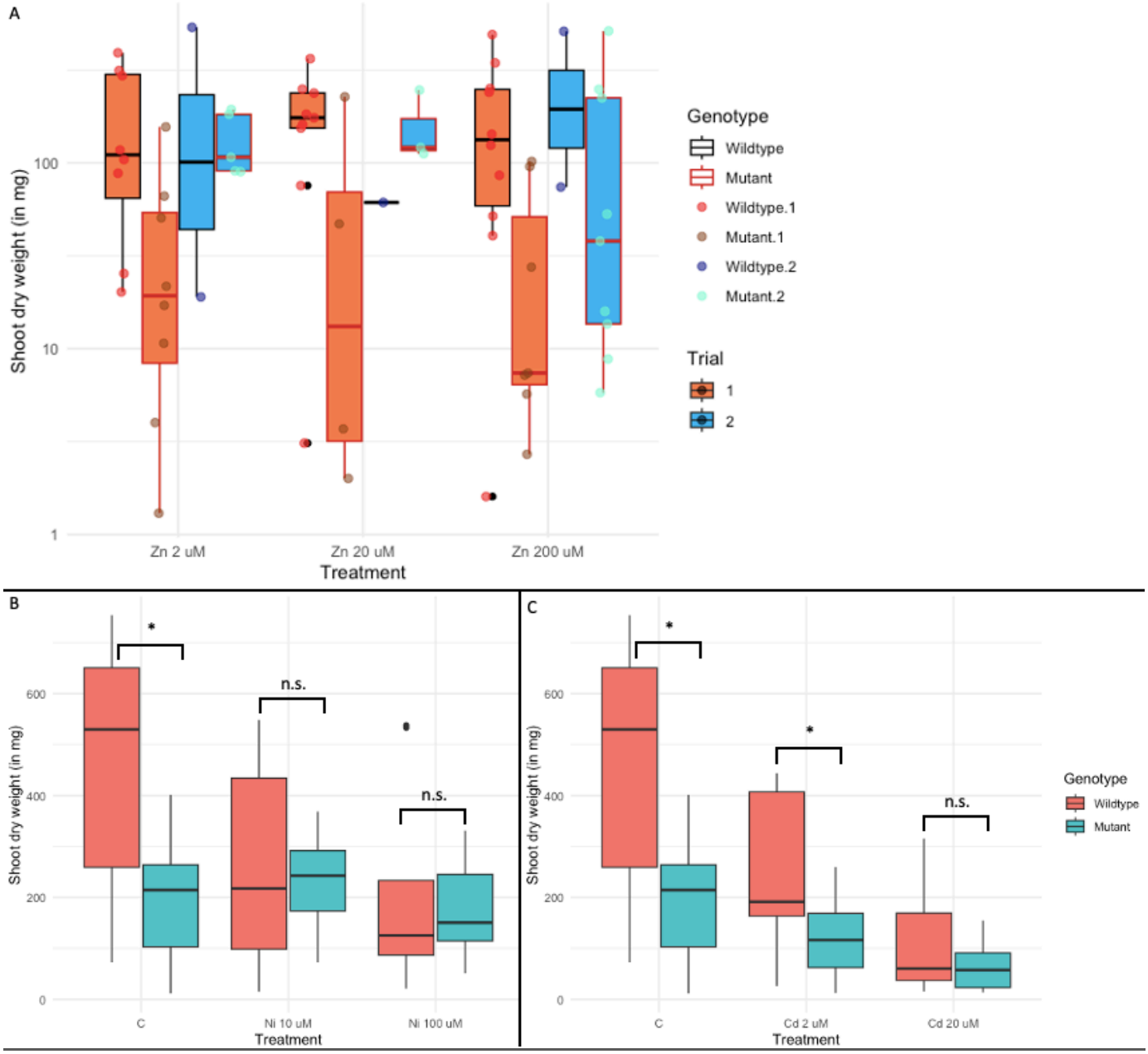

Appendix 6 Shoot dry weight in mg in *bzip19* mutant and *bZIP19* wildtype *N. caerulescens*.

A: Plants were treated with Zn. Two trials are shown. B: Plants were treated with Ni. "C" refers to the control treatment. * = p-value < 0.05, n.s. = not significant ($\alpha = 0.05$). p-value for Ni 0 µM (control), Ni 10 µM and Ni 100 µM is 0.021; 0.92; 0.75 respectively. C: Plants were treated with Cd. "C" refers to the control treatment. * = p-value < 0.05, n.s. = not significant ($\alpha = 0.05$). p-value for Cd 0 µM (control), Cd 2 µM and Cd 20 µM is 0.021; 0.025; 0.23 respectively.

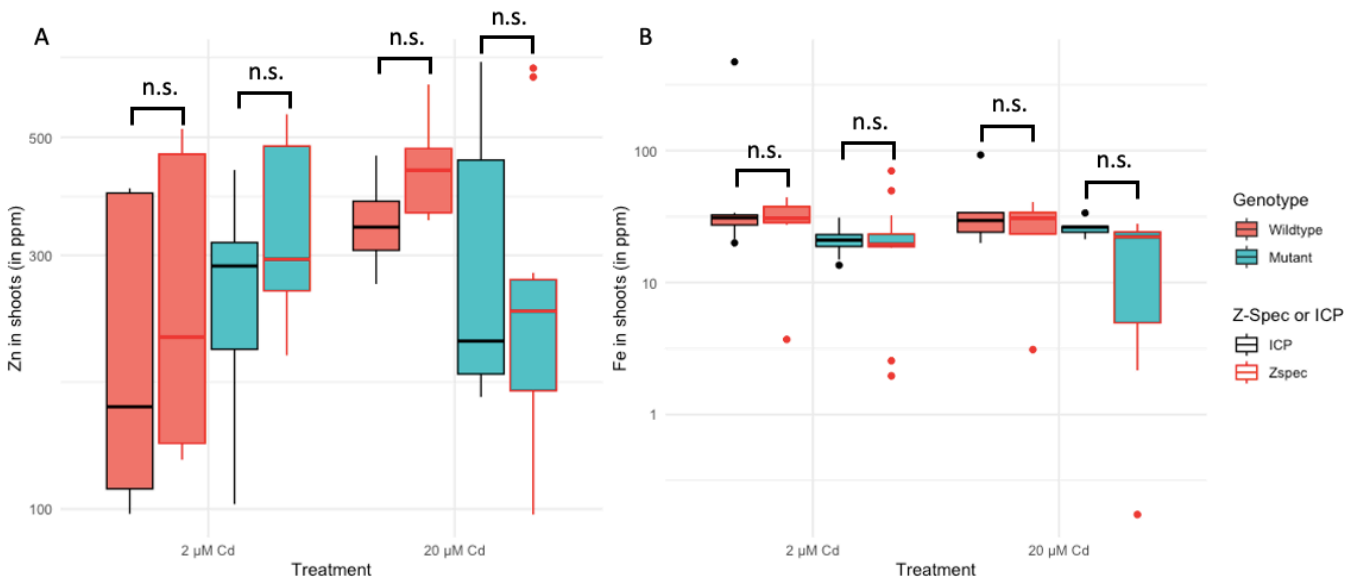

Appendix 7 Zn and Fe contents in bZIP19 wiltype and *bzip19* mutant *N. caerulescens* as measured via the Z-Spec or via ICP-AES.

Zn (A) and Fe (B) content are shown in ppm on a logarithmic scale for *N. caerulescens* shoots treated with 2 and 20 µM Cd. n.s. = not significant ($\alpha = 0.05$).